

Resource Allocation for the Training of Image Semantic Communication Networks

Yang Li, Xinyu Zhou, Jun Zhao

Abstract—Semantic communication is a new paradigm that aims at providing more efficient communication for the next-generation wireless network. It focuses on transmitting extracted, meaningful information instead of the raw data. However, deep learning-enabled image semantic communication models often require a significant amount of time and energy for training, which is unacceptable, especially for mobile devices. To solve this challenge, our paper first introduces a distributed image semantic communication system where the base station and local devices will collaboratively train the models for uplink communication. Furthermore, we formulate a joint optimization problem to balance time and energy consumption on the local devices during training while ensuring effective model performance. An adaptable resource allocation algorithm is proposed to meet requirements under different scenarios, and its time complexity, solution quality, and convergence are thoroughly analyzed. Experimental results demonstrate the superiority of our algorithm in resource allocation optimization against existing benchmarks and discuss its impact on the performance of image semantic communication systems.

Index Terms—Semantic communication, resource allocation, wireless communication, FDMA, convex optimization.

I. INTRODUCTION

Current information technologies near the Shannon capacity limits may not meet the rising data demands of the 6G era [1]. The upcoming 6G wireless technology is critical for emerging applications, e.g., Internet of Everything (IoE) [2], [3], virtual reality [4], autonomous driving [5], [6], wireless sensing [7], and other application domains [8]–[10]. To support these advances, this generation must offer high-speed, low-latency, and energy-efficient [11], [12] communication within the constraints of limited spectrum and power resources.

Semantic Communication (SemCom) [13] has attracted a lot of attention recently as a promising solution to the limitations of current information technologies. Unlike traditional methods that send all the data, SemCom is task-oriented and enables devices only to transmit desired semantic information extracted from the original data (i.e., text, image, and speech), thereby enhancing communication efficiency [14]. Compared

to textual data, the semantic information in an image is inherently implicit and depends on contextual knowledge. Hence, Deep Learning (DL) technology has been widely used in the image SemCom due to its advantage of deciphering the meaning of a figure. Specifically, the transmitter could use the DL model to encode the image into a low-dimensional vector to achieve highly efficient compression, which is then restored by the corresponding decoder at the receiver [15]. Furthermore, the learning capability of neural networks allows DL models to adjust to varying channel conditions, enhancing their ability to mitigate issues like noise interference.

Implementing DL-enabled image SemCom in a practical communication network also faces a shift from the current device-to-device manner to a sophisticated, network-centric system. Here, we consider a distributed image SemCom system, where each local device is equipped with a personalized DL-enabled SemCom model. During uplink communication, the local devices compress the image and transmit the semantic information. Upon reception, the base station decodes and recovers it. The system is continually trained to meet device requirements and changing channel conditions.

Motivation and Challenges. However, training a distributed image SemCom system within a real communication network presents several challenges: (1) **Power issue.** Although training DL models on local devices has become practical with the development in computation capability, the power issue has been a major concern, especially for mobile devices (i.e., phones and laptops). The training of DL models often brings a large amount of energy consumption on local devices, which may be unacceptable for users. (2) **Communication burden.** In the SemCom process, since the encoder and decoder are located on separate devices, this requires communication between the two devices (e.g., semantic information, model parameters, gradients) to complete the training. Due to the local devices' limited communication resources (e.g., transmission power, bandwidth), this process tends to result in high latency and energy costs. (3) **Device variability.** Different devices in the network may have different computing capabilities and individual requirements for SemCom (e.g., information compression rate). How to take into account this variability while ensuring effective training for each device is also a tricky problem.

To solve these challenges, we propose a DL-enabled image SemCom distributed system and aim to minimize the overall consumption to achieve more efficient training. The main **contributions** of our paper are summarized as follows:

- We propose a DL-enabled image SemCom system, where the local devices collaborate with the base station to train

Y. Li and X. Zhou are with the Graduate College at Nanyang Technological University (NTU), Singapore 639798. J. Zhao is with the College of Computing and Data Science (CCDS) at Nanyang Technological University (NTU), Singapore 639798. CCDS was formerly known as the School of Computer Science and Engineering (SCSE). Y. Li and X. Zhou are both NTU PhD students supervised by J. Zhao. (Emails: yang048@e.ntu.edu.sg, xinyu003@e.ntu.edu.sg, JunZhao@ntu.edu.sg)

Corresponding author: Jun Zhao.

This research is supported partly by Singapore Ministry of Education Academic Research Fund Tier 1 RT5/23, Tier 1 RG90/22, Nanyang Technological University (NTU)-Wallenberg AI, Autonomous Systems and Software Program (WASP) Joint Project, and Imperial-Nanyang Technological University Collaboration Fund INCF-2024-008.

real-time models, adapting to the varying channel conditions and optimizing model performance continuously.

- A joint optimization problem is formulated that aims to minimize a weighted sum of latency and energy consumption on local devices. We also investigate the relationship between model performance and relevant variables to guarantee the performance of SemCom.
- An adaptable resource allocation algorithm is developed. Owing to the problem’s intricate nature, non-convex ratios, and other complexities, we first decouple the original problem into tractable subproblems. Then, a tailored combination of the Lagrange function and a Newton-like approach is utilized to solve these subproblems. This algorithm dynamically adjusts to different system requirements. We also comprehensively analyze the time complexity, solution quality, and convergence.
- We implement extensive experiments to compare the proposed algorithm with benchmarks. Our results illustrate the superior performance of our algorithm in optimizing resource allocation while ensuring performance.

This paper is structured as follows: Section II reviews related work. Section III introduces the system model and notations. Section IV discusses problem formulation, followed by a proposed resource allocation algorithm in Section V. Section VI analyzes the algorithm’s performance. Simulation results are presented in Section VII, and the paper concludes with Section VIII.

II. LITERATURE REVIEW

This section surveys the literature on DL-enabled semantic communication techniques and resource allocation strategies in SemCom networks.

A. DL-enabled Semantic Communication Model

With the advent of powerful deep learning technologies, a number of studies have investigated the applications of DL-enabled semantic communication on text [16]–[19], images [20], [21], speech [22], and videos [23]. Specifically, Xie *et al.* [16] proposed DeepSC, a SemCom system using deep learning to maximize communication efficiency by minimizing semantic errors during text transmission. It employed a Transformer [24]-based architecture and further introduced transfer learning [25] to enhance adaptability across different communication environments. A new metric, sentence similarity, is also introduced to evaluate performance. Liu *et al.* [17] presented an Extended Context-based Semantic Communication (ECSC) system, enhancing text transmission by fully leveraging context information both within and between sentences. The ECSC encoder captures context with attention mechanisms, while the decoder uses Transformer-XL [26] for enhanced semantic recovery. Kutay *et al.* [18] utilized SBERT [27] to obtain sentence embeddings and a semantic distortion metric, preserving text meaning while achieving high compression results. They further integrate semantic quantization with semantic clustering, generalizing well across diverse text classification datasets. Peng *et al.* [19] introduced R-DeepSC, a robust deep learning-based system

using calibrated self-attention and adversarial training to mitigate the effects of “semantic noise” in text transmission. R-DeepSC outperforms traditional models only considering physical noise, demonstrating strong resilience to various signal-to-noise ratios.

Other than text, DL-enabled semantic communication also demonstrates satisfying performance on more complex data types (e.g., images and videos). For image transmission, Huang *et al.* [20] presented a Generative Adversarial Networks (GANs)-based image SemCom framework, achieving efficient semantic reconstructions. Lokumarambage *et al.* [21] proposed an end-to-end image SemCom system, using a pre-trained GAN at the receiver to reconstruct realistic images from semantic segmentation maps generated by the transmitter. In particular, the deployment of GAN allows it to combat noise in poor channel conditions, outperforming conventional compression methods. Grassucci *et al.* [22] proposed a generative audio semantic communication framework, employing a diffusion model to restore the received information from various degradations such as noise and missing parts. This approach focuses on semantic content rather than exact bitstream recovery, proving robustness to different channel conditions. For video transmission, Jiang *et al.* [23] introduced a semantic video conferencing (SVC) network where only critical frames of videos are transmitted, focusing on motions due to static backgrounds and infrequent speaker changes. Furthermore, they proposed an IR-HARQ framework with a semantic error detector and an SVC-CSI for channel feedback, improving error detection and transmission efficiency.

B. Resource Allocation in SemCom Networks

Most SemCom frameworks [16]–[23], [28] primarily focused on one-to-one device communication, and they often lack the adaptability required for large-scale scenarios. To bridge this gap, a number of recent studies [29]–[34] have shifted their focus towards developing both efficient and effective SemCom systems that are suitable for large-scale communication networks. Particularly, resource allocation acts as a significant factor in the above studies, as it is often crucial for improving the scalability and efficiency of networks, especially under resource-limited scenarios.

Those studies [29]–[34] concentrated on optimizing network resource allocation to enhance metrics such as latency, energy consumption and signal quality. Specifically, Yan *et al.* [29] introduced the concept of semantic spectral efficiency (S-SE), a novel metric designed to optimize resource allocation through strategic channel assignments and semantic symbol transmission. A semantic-aware resource allocation algorithm is also proposed to maximize the overall S-SE of all users. Afterward, they extended their work in a later study [30], developing an approximate measure of semantic entropy with a new quality-of-experience (QoE) model based on the measure. Resources, including symbol quantity, channel assignment and power allocation, are optimized to maximize the overall QoE. Wang *et al.* [31] presented a metric of semantic similarity (MSS), which can jointly capture the semantic accuracy and completeness of the recovered information. They integrated a

reinforcement learning (RL) algorithm and an attention-based network to optimize the resource allocation policy, maximizing the MSS of the whole network. Yang *et al.* [32] introduced a downlink SemCom network, minimizing overall energy usage by optimizing computation capacity, power control, rate allocation, etc. In addition, the SemCom model performance and latency are also considered constraints to the optimization problem. Zhang *et al.* [33] considered a task-oriented downlink SemCom network and aimed to enhance the overall transmission efficiency. A deep deterministic policy gradient (DDPG) agent is developed to optimize the balance between data delivery and task accuracy by managing the semantic compression ratio, transmit power, and bandwidth allocation. Zhang *et al.* [34] discussed an image SemCom network and aimed to minimize the average transmission latency of all users while satisfying the semantic reliability requirement. They managed to optimize resources such as user association, resource block (RB) allocation, and the selection of semantic information for transmission.

C. Comparison between Our Work and Related Studies

Previous related works [29]–[34] investigating resource allocation in SemCom networks mainly focused on the inference period rather than model training period in our study. There are also a few studies [35]–[37] discussing the training framework of SemCom networks, but they did not design the corresponding resource allocation strategy to optimize the system holistically. In synthesizing the above discussion, we highlight the unique contribution of our work: jointly optimizing latency, energy consumption and model performance while training an image SemCom network. We note that while several advancements exist in each domain, our integrated approach presents an innovative method that has yet to be fully explored in the existing literature.

III. SYSTEM MODEL

In this paper, we consider an image SemCom network consisting of one Base Station (BS) and a set of mobile devices: $\mathcal{N} = \{1, 2, \dots, N\}$. Due to the limited communication resources of mobile devices, they are required to perform SemCom during uplink image transmission. Given the varying channel conditions, the devices want to efficiently train their models for better SemCom performance. Hence, as illustrated in Fig. 1, we have developed a training system that allows mobile devices and the BS to jointly train their SemCom models. We first elaborate on our training paradigm in Section III-A, and then we discuss the consumption model and SemCom performance in Sections III-B and III-C, respectively.

A. Training of Semantic Communication Network

Semantic communication. In this paper, we utilize a DL-enabled model to achieve image SemCom. The main components are an encoder for image compression and a decoder for image reconstruction, as illustrated in the left side of Fig. 1. Next, we detail the components and the model objective.

Given an input image x , the encoder performs semantic encoding to extract relevant image features. Then, it further

transforms these features into a sequence of encoded symbols suitable for transmission, denoted as X . The whole encoder function could be expressed as follows:

$$X = f(x | \theta), \quad (1)$$

where $f(\cdot | \theta)$ represents the overall encoder function using a deep learning model parameterized by θ .

The encoded sequence X is transmitted through an AWGN channel, where it may encounter various disturbances. The corresponding output signal Y could be modeled as:

$$Y = X + \mathcal{N}^A, \quad (2)$$

where \mathcal{N}^A denotes the AWGN noise, which is a Gaussian random variable with zero mean and variance σ^2 .

After receiving signal Y , the encoder correspondingly performs channel decoding and semantic decoding, aiming to reconstruct the original image while minimizing distortion:

$$\hat{x} = f^{-1}(Y | \psi), \quad (3)$$

where \hat{x} is the reconstructed image and $f^{-1}(\cdot | \psi)$ denotes the decoder function with a model parameterized by ψ .

The objective of both the encoder and decoder is to jointly minimize the average distortion between the original image x and its reconstruction \hat{x} .

$$(\theta^*, \psi^*) = \arg \min_{\theta, \psi} \mathbb{E}[d(x, \hat{x})], \quad (4)$$

where $d(x, \hat{x})$ is the distortion measurement¹ of the x and \hat{x} .

In our considered scenario, the semantic communication models are deployed at both mobile devices and the BS. The devices utilize encoders to distill semantic information from images for uplink transmission. Upon reception, the BS reconstructs the images using the corresponding decoder. Specifically, we employ a deep joint source and channel coding (JSCC) model [38] as our SemCom model. The model aims to minimize the average mean squared error (MSE) loss between the original and reconstructed images. We defer a more detailed introduction of the model to Section III-A and describe below how to adapt it for training in our semantic communication network.

Iterative Training Method. We propose an iterative training method for our SemCom network, detailed in Algorithm 1. Following [16], [39], [40], we assume that both the mobile devices and the BS have access to a commonly shared training database. For simplicity, we denote the training data for a specific device n as Z_n , assuming that the data has been properly aligned between the devices and the BS beforehand. The process begins by setting a maximum number of iterations L and initializing the iteration counter $l = 0$. Each iteration l of the training process includes the following steps:

- Encoding and Transmission:
 - Each device n encodes its data Z_n into a semantic signal: $X_n = f(Z_n | \theta_n^l)$.
 - The signal X_n is then transmitted to the BS.
- Reception and Decoding at BS:
 - The BS receives signals $\mathbf{Y} = [Y_1, \dots, Y_N]$, where each $Y_n = X_n + \mathcal{N}_n^A$.
 - The BS decodes signals \mathbf{Y} using the decoder to obtain: $\hat{\mathbf{Z}} = [\hat{Z}_1, \dots, \hat{Z}_N]$, where $\hat{Z}_n = f^{-1}(Y_n | \psi_n^l)$.

¹Common measurements for image reconstruction include peak-signal-to-noise ratio (PSNR) and structural similarity index measure (SSIM), etc.

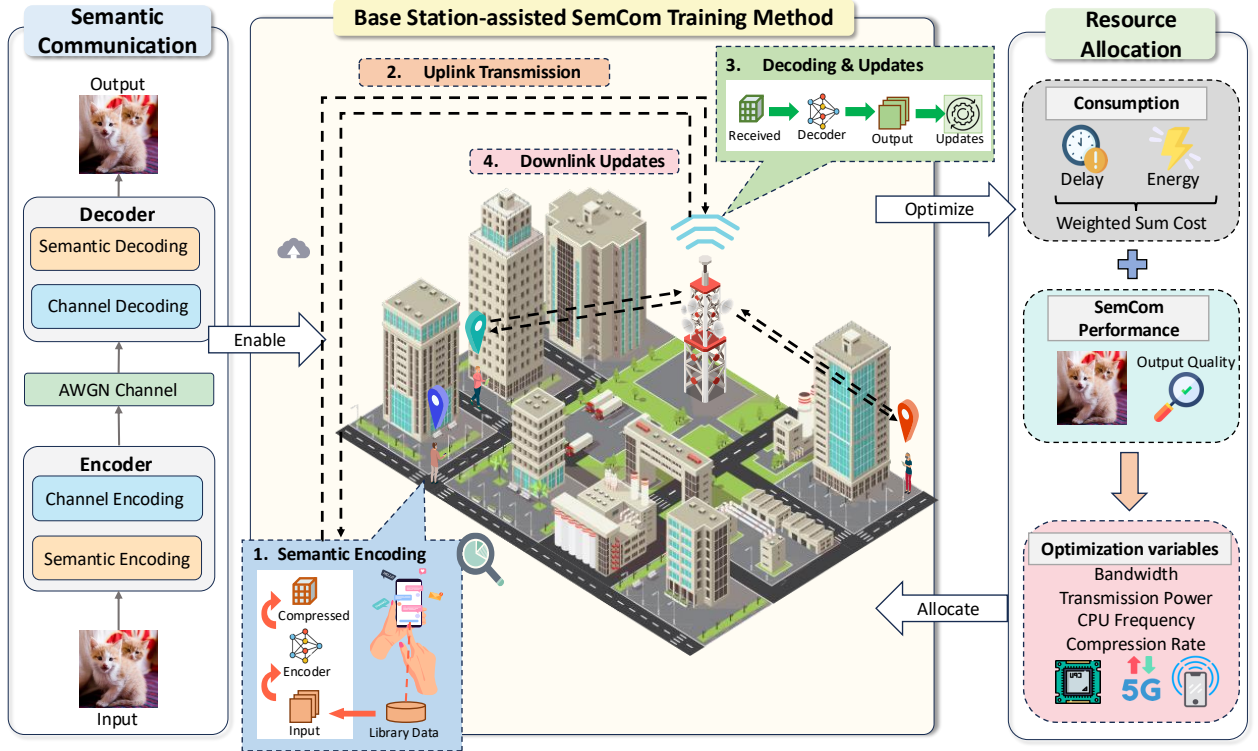


Fig. 1: System model.

- Loss Computation and Model Update:
 - The BS computes the MSE loss $\mathcal{L}_{\text{MSE}}(Z_n, \hat{Z}_n)$ to evaluate model performance of each device n .
 - The BS updates the whole model to $(\theta_n^{l+1}, \psi_n^{l+1})$ by applying the gradient descent on loss.
- Distribution of Updated Parameters:
 - The updated encoder θ_n^{l+1} is distributed back to each device n for local update.

Generally, Algorithm 1 is designed to continuously adapt the SemCom models to improve performance and robustness, accounting for channel conditions and device-specific data.

Algorithm 1: Iterative Training Method

Input: Models $\{(\theta_n^0, \psi_n^0) \mid n \in \mathcal{N}\}$;
 Training data $\mathbf{Z} = \{Z_n \mid n \in \mathcal{N}\}$;
Output: Trained models $\{(\theta_n^l, \psi_n^l) \mid n \in \mathcal{N}\}$.

- 1 Set maximum iterations L and iteration counter $l = 0$;
- 2 **while** $l \leq L$ or not convergence **do**
- 3 **for** each mobile device n in parallel **do**
- 4 $X_n \leftarrow f(Z_n \mid \theta_n^l)$;
- 5 Transmit X_n to the base station;
- 6 **for** BS to each device n in parallel **do**
- 7 Receive signal Y_n , where $Y_n = X_n + \mathcal{N}_n^A$;
- 8 $\hat{Z}_n \leftarrow f^{-1}(Y_n \mid \psi_n^l)$;
- 9 Compute the MSE loss: $\mathcal{L}_{\text{MSE}}(Z_n, \hat{Z}_n)$;
- 10 Update the whole model:
 $(\theta_n^{l+1}, \psi_n^{l+1}) \leftarrow (\theta_n^l, \psi_n^l) - \eta \cdot \nabla_{\theta_n^l, \psi_n^l} \mathcal{L}_{\text{MSE}}(Z_n, \hat{Z}_n)$;
- 11 Distribute θ_n^{l+1} to each device n ;
- 12 Let $l \leftarrow l + 1$;

TABLE I: Notations.

Description	Symbol
The number of total devices	N
Original data on device n	Z_n
Reconstructed data at the base station	\hat{Z}_n
Encoder and decoder of device n	θ_n, ψ_n
Encoded signal of device n	X_n
Channel output of device n	Y_n
Total available bandwidth	B_{total}
Allocated bandwidth to device n	B_n
The power density of Gaussian noise	N_0
The number of CPU cycles per sample on device n	c_{1n}
The number of CPU cycles per sample on the BS	c_{2n}
The number of samples on device n	D_n
Local computation frequency of device n	f_n
Allocated frequency to device n on the BS	h_n
Transmission power of device n	p_n
Uplink transmission rate	r_n
Signal-to-Noise Ratio	S_n
Local computation time on device n	T_n^{cmp}
Uplink transmission time on device n	T_n^{up}
The effective switched capacitance	κ
Size of per sample data on device n	d_n
Compression rate of semantic communication	ρ_n
Local computation energy of device n	E_n^{cmp}
Uplink transmission energy of device n	E_n^{up}
Overall energy consumption among devices	E
Weight parameters for time and energy	ω_1, ω_2
Maximum transmission power	p_n^{max}
Maximum frequency on device n	f_n^{max}
Maximum allocated frequency to device n on the BS	h_n^{max}
Maximum transmission power	p_n^{max}
Maximum and minimum compression rate	$\rho_n^{\text{max}}, \rho_n^{\text{min}}$
Minimum PSNR requirement of device n	F_n^{min}

B. Computation and Transmission Model

In this subsection, we give a detailed introduction to our computation and transmission model within the SemCom system. Considering the BS usually possesses abundant communication resources (e.g., high transmission power and abundant bandwidth), our primary focus lies in minimizing the consumption of mobile devices and the computation consumption of the BS [41]–[44]. We first introduce the frequency division multiplexing technique used, followed by the formulation of time completion as well as energy consumption.

FDMA. Following [41], [42], [45], we adopt FDMA technology, which could be implemented simply for mobile devices with limited computation capability [46]. Specifically, given a total bandwidth B_{total} , the bandwidth allocated to each user n is denoted as B_n , and $\sum_{n=1}^N B_n \leq B_{\text{total}}$.

Time consumption of mobile devices. In each training iteration, mobile device n encodes the original image data and then transmits the encoded signal to the BS. Hence, we first analyze the computation time consumption for encoding. Assuming that the CPU frequency f_n does not change over time until it has been optimized, the computation time on device n is:

$$T_n^{\text{cmp}} = \frac{c_{1n}D_n}{f_n}, \quad (5)$$

where c_{1n} and D_n are the required CPU cycles per sample and the number of samples on device n , respectively. Based on the Shannon formula, we define the uplink transmission rate of device n as follows:

$$r_n = B_n \log_2 \left(1 + \frac{p_n g_n}{N_0 B_n} \right), \quad (6)$$

where p_n is the transmission power, g_n is the channel gain and N_0 is the power spectral density of Gaussian noise. Let d_n represent the size of per sample on device n , with a semantic information compression rate of ρ_n . According to Algorithm 1, the uplink transmission time T_n^{up} of device n is:

$$T_n^{\text{up}} = \frac{\rho_n d_n D_n}{r_n}, \quad (7)$$

where ρ_n is the compression rate and is defined as the ratio of the size of semantic information to that of the original data. Thereafter, the overall time consumption T_n^D on device n in one iteration is expressed as:

$$T_n^D = T_n^{\text{cmp}} + T_n^{\text{up}}. \quad (8)$$

Time consumption of the BS. Upon receiving the encoded signal, the BS decodes it for reconstruction and updates the SemCom model. The updated model is finally sent back to each device n . Since computation consumption is the main source of overhead, we define the BS's time corresponding to each device n as follows:

$$T_n^S = \frac{c_{2n}D_n}{h_n}, \quad (9)$$

where c_{2n} denotes the required CPU cycles for decoding and model updating per sample, and h_n is the assigned frequency to device n on the BS.

Energy consumption of mobile devices. Following [43], we define the computation energy consumption of device n during one round of training as follows:

$$E_n^{\text{cmp}} = \kappa c_{1n} D_n f_n^2, \quad (10)$$

where κ denotes the effective capacitance coefficient. Since the transmission time T_n^{up} is already obtained in (7), the

transmission energy consumption E_n^{up} could be formulated as:

$$E_n^{\text{up}} = p_n T_n^{\text{up}} = p_n \frac{\rho_n d_n D_n}{r_n}. \quad (11)$$

Hence, the overall energy consumption of device n is:

$$E_n^D = E_n^{\text{cmp}} + E_n^{\text{up}}. \quad (12)$$

Energy consumption of the BS. Based on computation time T_n^S in (9), we define E_n^S as the BS's energy consumption corresponding to each device n :

$$E_n^S = \kappa c_{2n} D_n h_n^2. \quad (13)$$

C. SemCom Performance Analysis

We employ the Peak Signal-to-Noise Ratio (PSNR) metric to evaluate the performance of the image SemCom model. PSNR is computed from the MSE loss and indicates the similarity between the original and reconstructed images at the pixel level [20], [47]–[49]. In our scenario, given the SemCom models, we examine PSNR's dependence on two key factors: the semantic information compression rate ρ_n and the Signal-to-noise ratio (SNR) S_n , where $S_n = \frac{p_n g_n}{N_0 B_n}$. Higher values of ρ_n and S_n improve the quality of the reconstructed image, as they mitigate information loss caused by compression and enhance transmission reliability. Based on the observed characteristics of PSNR in SemCom [38] and other practical applications [50], [51], the PSNR value can be modeled as a concave function $P(\cdot)$ concerning ρ_n and S_n . Hence, we make an assumption of $P(\rho_n, S_n)$ that is presented in Condition 1.

Condition 1. The PSNR function $P(\rho_n, S_n)$ for any $n \in \mathcal{N}$ is concave and non-decreasing with respect to $\rho_n > 0$ and $S_n > 0$; i.e., $P''(x) < 0$ and $P'(x) > 0$ for $x > 0$, where x denotes ρ_n or S_n .

The concavity of $P(\rho_n, S_n)$ means diminishing marginal gain. For the specific expression of $P(x)$ used in the experiments, we will discuss it in Section VII-B.

IV. JOINT OPTIMIZATION PROBLEM FORMULATION

In this section, we begin with formulating the joint optimization problem, followed by a discussion on the challenges and strategies for solving it.

A. Problem Formulation

The training of the SemCom network can cause considerable overhead to mobile devices and the base station. Due to limited resources, one of our goals is to minimize the overall time consumption in one training iteration:

$$\min \left\{ \max_{n \in \mathcal{N}} \{T_n\} \right\}, \quad (14)$$

where $T_n = T_n^D + T_n^S$ denotes device n 's total training time consumption. The max operation in (14) is for fairness (i.e., devices that become ‘‘bottlenecks’’ in time consumption will be continuously optimized). Concurrently, we also aim to minimize the overall energy consumption within the network:

$$\min \left\{ \sum_{n=1}^N E_n \right\}, \quad (15)$$

where $E_n = E_n^D + E_n^S$ denotes each device n 's total energy consumption. Synthesizing the above two objectives (14) and

(15), a joint optimization problem can be formulated as follows:

$$\mathbb{P}_1 : \min_{\mathbf{p}, \mathbf{B}, \mathbf{f}, \mathbf{h}, \rho} \left\{ \omega_1 \max_{n \in \mathcal{N}} \{T_n\} + \omega_2 \sum_{n=1}^N E_n \right\}, \quad (16)$$

$$\text{s.t. : } p_n \leq p_n^{\max}, \quad \forall n \in \mathcal{N}, \quad (16a)$$

$$f_n \leq f_n^{\max}, \quad \forall n \in \mathcal{N}, \quad (16b)$$

$$\sum_{n=1}^N B_n \leq B_{\text{total}}, \quad (16c)$$

$$h_n \leq h_n^{\max}, \quad \forall n \in \mathcal{N} \quad (16d)$$

$$P_n^{\min} \leq P_n(\rho_n, S_n(p_n, B_n)), \quad \forall n \in \mathcal{N}, \quad (16e)$$

$$\rho_n^{\min} \leq \rho_n \leq \rho_n^{\max}, \quad \forall n \in \mathcal{N}, \quad (16f)$$

where $\omega_1, \omega_2 \in [0, 1]$ are weights for time and energy consumption, respectively, and we can enforce $\omega_1 + \omega_2 = 1$ after normalization. Constraints (16a) and (16b) set the ranges of transmission power and computation frequency for each device n . Constraint (16c) imposes an upper limit on the total available uplink bandwidth. Constraint (16d) sets the maximum available computation resources for each device n at the BS. P_n^{\min} in constraint (16e) is the required minimum model accuracy for device n , and constraint (16f) sets the range of values for the compression rate.

B. Challenges and Strategies of Solving Problem \mathbb{P}_1

Problem \mathbb{P}_1 has a complex construction form and is subject to complicated constraints (16a)-(16f). In the objective function, both T_n^{up} and E_n^{up} are non-convex and compound p_n, B_n, ρ_n three variables, making them extremely complex. The presence of the max function further complicates the problem-solving process. Besides, the joint concavity of $A_n(\rho_n, S_n)$ in constraint (16e) with respect to ρ_n and S_n is also not guaranteed, as we discuss in Section III-C.

To streamline the problem \mathbb{P}_1 for efficient resolution, we first introduce an auxiliary variable \mathcal{T} . This variable replaces the time completion T in (16), accompanied by an additional constraint. Consequently, we reformulate \mathbb{P}_1 as follows:

$$\mathbb{P}_2 : \min_{\mathbf{p}, \mathbf{B}, \mathbf{f}, \rho, \mathcal{T}} \left\{ \omega_1 \mathcal{T} + \omega_2 \sum_{n=1}^N E_n \right\}, \quad (17)$$

$$\text{s.t. : } (16a), (16b), (16c), (16d), (16e), (16f),$$

$$T_n^{\text{up}} + T_n^{\text{cmp}} + T_n^S \leq \mathcal{T}, \quad \forall n \in \mathcal{N}. \quad (17a)$$

However, the problem of T_n^{up} and E_n^{up} being non-convex and $A_n(\rho_n, S_n)$ being non-concave remains unsolved. Considering that they are coupled with several variables, we decompose \mathbb{P}_2 into two subproblems for further simplification. Since $A_n(\rho_n, S_n)$ is not guaranteed to be jointly concave with respect to ρ_n and S_n , and variables p_n and B_n appear together in the term $S_n = \frac{p_n g_n}{N_0 B_n}$, \mathbb{P}_3 involves optimization variables f_n, ρ_n and \mathcal{T} , while \mathbb{P}_4 involves variables p_n and B_n .

$$\mathbb{P}_3(\mathbf{p}, \mathbf{B}) : \min_{\mathbf{f}, \rho, \mathbf{h}, \mathcal{T}} \left\{ \omega_1 \mathcal{T} + \omega_2 \sum_{n=1}^N (E_n^{\text{cmp}} + E_n^S) \right\}, \quad (18)$$

$$\text{s.t. : } (16b), (16d), (16e), (16f), (17a).$$

$$\mathbb{P}_4(\mathbf{f}, \rho, \mathcal{T}) : \min_{\mathbf{p}, \mathbf{B}} \left\{ \omega_2 \sum_{n=1}^N E_n^{\text{up}} \right\}, \quad (19)$$

$$\text{s.t. : } (16a), (16c), (16e), (17a).$$

To solve problem \mathbb{P}_1 , we adopt the following alternating optimization process:

- given \mathbf{p} and \mathbf{B} , we solve \mathbb{P}_3 to optimize $\mathbf{f}, \mathbf{h}, \rho$, and \mathcal{T} .
- given $\mathbf{f}, \mathbf{h}, \rho$, and \mathcal{T} , we solve \mathbb{P}_4 to optimize \mathbf{p} and \mathbf{B} .

It is worth noting that despite the decomposition, \mathbb{P}_4 is still a challenging pseudoconvex ratio as validated by Lemma 1:

Lemma 1. For Problem \mathbb{P}_4 , we have:

- Rate r_n is jointly concave with respect to p_n and B_n ;
- Ratio $\frac{p_n \rho_n d_n}{r_n}$ in E_n^{up} is jointly pseudoconvex with regard to p_n and B_n .

Proof. For the rate r_n as a function of p_n and B_n , we calculate the Hessian matrix as follows:

$$H = \begin{bmatrix} -\frac{g_n^2}{B_n N_0^2 (1 + \frac{p_n g_n}{N_0 B_n})^2 \ln 2} & \frac{p_n g_n^2}{B_n^3 N_0^2 (1 + \frac{p_n g_n}{N_0 B_n})^2 \ln 2} \\ \frac{p_n g_n^2}{B_n^2 N_0^2 (1 + \frac{p_n g_n}{N_0 B_n})^2 \ln 2} & -\frac{p_n^2 g_n^2}{B_n^3 N_0^2 (1 + \frac{p_n g_n}{N_0 B_n})^2 \ln 2} \end{bmatrix}$$

Then for any vector $x = [x_1, x_2]^T \in \mathbb{R}^2$, we obtain $x^T H x = -\frac{(x_1 B_n - x_2 p_n)^2 g_n^2}{B_n^3 N_0^2 (1 + \frac{p_n g_n}{N_0 B_n})^2 \ln 2} \leq 0$, so H is a negative semidefinite matrix, which means that $r_n(p_n, B_n)$ is a jointly concave function. Besides, $p_n \rho_n d_n$ is an affine function with p_n . Referring to Page 245 of the book [52], the ratio is deemed pseudoconvex when the numerator satisfies the properties of being non-negative, concave, and differentiable, and the denominator satisfies the properties of being positive, convex, and differentiable. Thus, Lemma 1 is proved. \square

Remark 1. Based on the proof of Lemma 1, $\frac{p_n \rho_n d_n}{r_n}$ is jointly pseudoconvex and can also be referred to as a concave-convex ratio, marked by a concave numerator and a convex denominator. Unfortunately, the sum of pseudoconvex functions does not inherently retain pseudoconvexity, presenting a challenge in solving such sum-of-ratio problems [53]–[55].

To address the sum of pseudoconvex ratios problem in \mathbb{P}_4 , a Newton-like method will be introduced in Section V-B. Generally, our strategy entails the initial random selection of feasible (\mathbf{p}, \mathbf{B}) , followed by solving \mathbb{P}_3 to obtain the optimal solutions \mathbf{f}^*, ρ^* and \mathcal{T}^* . Subsequently, we solve \mathbb{P}_4 to derive the optimal \mathbf{p}^* and \mathbf{B}^* . Optimums to \mathbb{P}_2 progressively converge through the iterative resolution of \mathbb{P}_3 and \mathbb{P}_4 .

V. SOLUTIONS TO THE JOINT OPTIMIZATION PROBLEM

In this section, we will solve subproblems \mathbb{P}_3 and \mathbb{P}_4 , and then present a resource allocation algorithm.

A. Solution to \mathbb{P}_3

To solve problem \mathbb{P}_3 more efficiently, we first define $\bar{\rho}_n(p_n, B_n)$ such that $P_n(\bar{\rho}_n, S_n(p_n, B_n)) = P_n^{\min}$. Then constraint (16e) is equivalent to

$$\rho_n \geq \bar{\rho}_n(p_n, B_n). \quad (20)$$

Considering constraint (16f) to the compression rate, we have:

- If $\bar{\rho}_n(p_n, B_n) > \rho_n^{\max}$, then $\mathbb{P}_3(\mathbf{p}, \mathbf{B})$ has no solution.

- If $\bar{\rho}_n(p_n, B_n) \leq \rho_n^{\max}$, then the solution $\boldsymbol{\rho}$ is given by $\boldsymbol{\rho}^*(\mathbf{p}, \mathbf{B})$, whose n -th dimension is $\rho_n^*(p_n, B_n) := \max\{\bar{\rho}_n(p_n, B_n), \rho_n^{\min}\}$ according to (16f) and (20).

After obtaining the optimal $\boldsymbol{\rho}^*$, we can simplify original problem \mathbb{P}_3 into the following:

$$\mathbb{P}_5(\mathbf{p}, \mathbf{B}, \boldsymbol{\rho}^*) : \min_{\mathbf{f}, \mathbf{h}, \mathcal{T}} \left\{ \omega_1 \mathcal{T} + \omega_2 \sum_{n=1}^N (E_n^{\text{cmp}} + E_n^S) \right\}, \quad (21)$$

s.t. : (16b), (16d),

$$T_n^{\text{up}} + T_n^{\text{cmp}}(f_n) + T_n^S(h_n) \leq \mathcal{T}, \quad \forall n \in \mathcal{N}. \quad (21a)$$

When both the objective function and constraints of a minimization problem are convex, it constitutes a convex optimization problem, leading to the following lemma:

Lemma 2. *For a convex optimization problem, the Karush–Kuhn–Tucker (KKT) conditions are*

- sufficient to find the optimum, and
- are necessary for optimality if at least one of the regularity conditions² holds.

Proof. Please refer to chapters 5.2.3 and 5.5.3 of [56]. \square

It is easy to verify \mathbb{P}_5 is a convex optimization problem with variables $(\mathbf{f}, \mathbf{h}, \mathcal{T})$ and satisfy Slater's condition³. One viable approach to solve it is to employ the KKT conditions directly. Then for \mathbb{P}_3 , with $\boldsymbol{\alpha} := [\alpha_n |_{n \in \mathcal{N}}]$ and $\boldsymbol{\beta} := [\beta_n |_{n \in \mathcal{N}}]$ denoting the multiplier, the Lagrangian function is given by:

$$\begin{aligned} \mathcal{L}_1(\mathbf{f}, \mathbf{h}, \mathcal{T}, \boldsymbol{\alpha}, \boldsymbol{\tau}, \boldsymbol{\beta}) &= \omega_1 \mathcal{T} + \omega_2 \sum_{n=1}^N \kappa D_n (c_{1n} f_n^2 + c_{2n} h_n^2) \\ &+ \sum_{n=1}^N \alpha_n (f_n - f_n^{\max}) + \sum_{n=1}^N \tau_n (h_n - h_n^{\max}) \\ &+ \sum_{n=1}^N \beta_n (T_n^{\text{up}} + T_n^{\text{cmp}}(f_n) + T_n^S(h_n) - \mathcal{T}). \end{aligned} \quad (22)$$

The KKT conditions are as follows, where we abbreviate $\mathcal{L}_1(\mathbf{f}, \mathbf{h}, \mathcal{T}, \boldsymbol{\alpha}, \boldsymbol{\nu}, \boldsymbol{\beta})$ as \mathcal{L}_1 :

Stationarity:

$$\frac{\partial \mathcal{L}_1}{\partial f_n} = 2\omega_2 \kappa c_{1n} D_n f_n + \alpha_n - \beta_n \frac{c_{1n} D_n}{f_n^2} = 0, \quad (23a)$$

$$\frac{\partial \mathcal{L}_1}{\partial h_n} = 2\omega_2 \kappa c_{2n} D_n h_n + \tau_n - \beta_n \frac{c_{2n} D_n}{h_n^2} = 0, \quad (23b)$$

$$\frac{\partial \mathcal{L}_1}{\partial \mathcal{T}} = \omega_1 - \sum_{n=1}^N \beta_n = 0. \quad (23c)$$

Complementary Slackness:

$$\alpha_n \cdot (f_n - f_n^{\max}) = 0, \quad (24a)$$

$$\tau_n \cdot (h_n - h_n^{\max}) = 0, \quad (24b)$$

$$\beta_n \cdot (T_n^{\text{up}} + T_n^{\text{cmp}} + T_n^S - \mathcal{T}) = 0. \quad (24c)$$

Primal feasibility: (16b), (16d), (17a).

Dual feasibility:

$$(25a): \alpha_n \geq 0, \quad (25b): \tau_n \geq 0, \quad (25c): \beta_n \geq 0.$$

²Regularity conditions refer to a variety of constrained conditions under which a minimizer point x^* of the original optimization problem has to satisfy the KKT conditions.

³In brief, Slater's condition means that the feasible set of the optimization problem contains at least one interior point which makes all the inequality constraints *strictly* hold [56].

To find the optimal solution $(\mathbf{f}^*, \mathbf{h}^*, \mathcal{T}^*)$ for \mathbb{P}_3 , we analyze the KKT conditions step by step. We first compute f_n and h_n as functions of β_n by setting $\alpha_n = 0$ and $\nu_n = 0$:

$$\bar{f}_n(\beta_n) = \sqrt[3]{\frac{\beta_n}{2\omega_2 \kappa}}, \quad (26)$$

$$\bar{h}_n(\beta_n) = \sqrt[3]{\frac{\beta_n}{2\omega_2 \kappa}}. \quad (27)$$

We first analyze f_n and discuss the following two cases:

- **Case 1:** $\bar{f}_n(\beta_n) \leq f_n^{\max}$. In this case, we simply set $\alpha_n = 0$ and $f_n^* = \bar{f}_n(\beta_n)$.
- **Case 2:** $\bar{f}_n(\beta_n) > f_n^{\max}$. Setting $\alpha_n = 0$ is not feasible, as it leads to $f_n^* = \bar{f}_n(\beta_n)$ from (23a) and violates the primal feasibility constraint (16b). Therefore, with $\alpha_n > 0$ in Equation (24a), we conclude $f_n = f_n^{\max}$.

Summarize the above cases, and we have:

$$f_n^*(\beta_n) = \min\{\bar{f}_n(\beta_n), f_n^{\max}\}. \quad (28)$$

The analysis of h_n is similar to that of f_n . Hence, we could also have:

$$h_n^*(\beta_n) = \min\{\bar{h}_n(\beta_n), h_n^{\max}\}. \quad (29)$$

According to (23a), only $\beta_n > 0$ could make the equality hold. Substituting $\beta_n > 0$ in (24c), we could derive that:

$$T_n^{\text{up}} + T_n^{\text{cmp}}(f_n^*(\beta_n)) + T_n^S(h_n^*(\beta_n)) = \mathcal{T}. \quad (30)$$

Based on (30), we could compute β_n as a function of \mathcal{T} , denoted as $\beta_n(\mathcal{T})$. Then, we substitute $\beta_n(\mathcal{T})$ into (23c):

$$\sum_{n=1}^N \beta_n(\mathcal{T}) = \omega_1. \quad (31)$$

It is easy to verify that the left part of (31) is monotonic with respect to \mathcal{T} , thus a bisection method is sufficient to solve it and derive the optimal \mathcal{T}^* . Subsequently, \mathbf{f}^* and \mathbf{h}^* could also be derived. Thus, the optimal solution to \mathbb{P}_3 is as follows:

$$\begin{cases} \mathcal{T}^* = \text{Solution to (31)}, \\ \rho_n^* = \max\{\bar{\rho}_n(p_n, B_n), \rho_n^{\min}\}, \\ f_n^* = \min\{\bar{f}_n(\beta_n^*), f_n^{\max}\}, \\ h_n^* = \min\{\bar{h}_n(\beta_n^*), h_n^{\max}\}. \end{cases} \quad (32)$$

B. Solution to SUB2

Problem \mathbb{P}_4 represents a typical sum-of-ratios problem. Given the challenges in analyzing the pseudoconvexity of the objective function $\sum_{n=1}^N E_n^{\text{up}}$ in \mathbb{P}_4 , we will utilize a more efficient fractional programming method to solve it. Initially, we use $r_n(p_n, B_n)$ to denote $B_n \log_2(1 + \frac{p_n g_n}{N_0 B_n})$ for simplicity and constraint (17a) could be rewritten as $r_n^{\min} \leq r_n(p_n, B_n)$, where $r_n^{\min} = \frac{\mathcal{T}^* - T_n^{\text{cmp}} - T_n^S}{\rho_n d_n}$, and constraint (16e) could be simplified as $S_n^{\min} \leq \frac{p_n g_n}{N_0 B_n}$, where $S_n^{\min} = A_n^{-1}(P_n^{\min}, \rho_n^*)$.

Furthermore, we introduce an auxiliary variable δ_n to transform problem \mathbb{P}_4 into an epigraph form. Through introducing an additional constraint $\frac{p_n \rho_n d_n D_n}{r_n(p_n, B_n)} \leq \delta_n$, we can convert \mathbb{P}_4 into the equivalent \mathbb{P}_6 :

$$\mathbb{P}_6(\mathbf{f}, \mathbf{h}, \boldsymbol{\rho}, \mathcal{T}) : \min_{\mathbf{p}, \mathbf{B}, \boldsymbol{\delta}} \left\{ \omega_2 \sum_{n=1}^N \delta_n \right\}, \quad (33)$$

s.t. : (16a), (16c),

$$r_n^{\min} - r_n(p_n, B_n) \leq 0, \quad (33a)$$

$$N_0 B_n S_n^{\min} - p_n g_n \leq 0, \quad (33b)$$

$$p_n \rho_n d_n D_n - \delta_n r_n(p_n, B_n) \leq 0. \quad (33c)$$

However, \mathbb{P}_6 is still a non-convex problem since $\delta_n r_n(p_n, B_n)$ in (33c) is not jointly convex. Thus, we manage to further transform problem \mathbb{P}_6 into a convex problem \mathbb{P}_7 through the following theorem.

Theorem 1. *If $(\mathbf{p}^*, \mathbf{B}^*, \boldsymbol{\xi}^*)$ is the globally optimal solution of \mathbb{P}_6 , then there exist $(\boldsymbol{\gamma}^*, \boldsymbol{\delta}^*)$ such that $(\mathbf{p}^*, \mathbf{B}^*)$ is a solution of the following problem for $\boldsymbol{\gamma} = \boldsymbol{\gamma}^*$ and $\boldsymbol{\delta} = \boldsymbol{\delta}^*$.*

$$\mathbb{P}_7(\mathbf{f}, \mathbf{h}, \boldsymbol{\rho}, \mathcal{T}) : \min_{\mathbf{p}, \mathbf{B}} \left\{ \sum_{n=1}^N \gamma_n \cdot (p_n \rho_n d_n D_n - \delta_n r_n(p_n, B_n)) \right\}, \quad (34)$$

s.t. : (16a), (16c), (33a), (33b).

Furthermore, $(\mathbf{p}^*, \mathbf{B}^*)$ also satisfies the following equations under the conditions of $\boldsymbol{\gamma} = \boldsymbol{\gamma}^*$ and $\boldsymbol{\delta} = \boldsymbol{\delta}^*$:

$$\gamma_n^* = \frac{\omega_2}{r_n(p_n^*, B_n^*)}, \quad (35a)$$

$$\text{and } \delta_n^* = \frac{p_n^* \rho_n d_n D_n}{r_n(p_n^*, B_n^*)}. \quad (35b)$$

Proof. The proof is given by Lemma 2.1 in [53]. \square

Theorem 1 indicates that problem \mathbb{P}_7 has the same optimal solution with \mathbb{P}_6 . Intuitively, we next focus on how to derive the optimal $(\boldsymbol{\delta}^*, \boldsymbol{\gamma}^*)$ to solve \mathbb{P}_7 . We employ an alternating optimization approach to optimize the two sets of variables $(\boldsymbol{\delta}, \boldsymbol{\gamma})$ and (\mathbf{p}, \mathbf{B}) , which is described in **Algorithm 2**.

Algorithm 2 starts by calculating the initial values of auxiliary variables $(\boldsymbol{\delta}^{(0)}, \boldsymbol{\gamma}^{(0)})$ based on (37). Then, during the i -th iteration of Algorithm 2, $(\boldsymbol{\delta}^{(i)}, \boldsymbol{\gamma}^{(i)})$ are updated to $(\boldsymbol{\delta}^{(i+1)}, \boldsymbol{\gamma}^{(i+1)})$ based on (39)-(42), which states the modified Newton method to solve $\phi(\boldsymbol{\delta}, \boldsymbol{\gamma}) = 0$ until convergence or reaching maximum iteration number I .

Next, our attention turns to solving \mathbb{P}_7 when $\boldsymbol{\gamma}$ and $\boldsymbol{\delta}$ are obtained from Algorithm 2. Noting that \mathbb{P}_7 is inherently a convex problem, KKT conditions can be utilized to solve it. Specifically, the Lagrange function of (34) could be given by:

$$\begin{aligned} \mathcal{L}_2(\mathbf{p}, \mathbf{B}, \zeta, \boldsymbol{\eta}, \boldsymbol{\nu}, \boldsymbol{\iota}) &= \sum_{n=1}^N \gamma_n \cdot (p_n \rho_n d_n D_n - \delta_n r_n(p_n, B_n)) \\ &+ \zeta \cdot \left(\sum_{n=1}^N B_n - B_{\text{total}} \right) + \sum_{n=1}^N \eta_n \cdot (r_n^{\min} - r_n(p_n, B_n)) \\ &+ \sum_{n=1}^N \nu_n \cdot (N_0 B_n S_n^{\min} - p_n g_n) + \sum_{n=1}^N \iota_n \cdot (p_n - p_n^{\max}). \end{aligned} \quad (43)$$

where $\zeta, \boldsymbol{\eta}, \boldsymbol{\iota}$ and $\boldsymbol{\nu}$ are non-negative Lagrangian multipliers. The corresponding KKT conditions as follows:

Stationarity:

$$\frac{\partial \mathcal{L}_2}{\partial p_n} = \gamma_n \rho_n d_n D_n - \frac{(\gamma_n \delta_n + \eta_n) g_n}{N_0(1 + S_n) \ln 2} - \nu_n g_n + \iota_n = 0, \quad (44a)$$

$$\begin{aligned} \frac{\partial \mathcal{L}_2}{\partial B_n} &= -(\gamma_n \delta_n + \eta_n) \log_2(1 + S_n) + \frac{(\gamma_n \delta_n + \eta_n) S_n}{(1 + S_n) \ln 2} \\ &+ \zeta + \nu_n N_0 S_n^{\min} = 0. \end{aligned} \quad (44b)$$

where $S_n = \frac{p_n g_n}{N_0 B_n}$ for simplicity.

Algorithm 2: Refinement of Parameters (\mathbf{p}, \mathbf{B})

Input: Initial feasible solution $(\mathbf{p}^{(0)}, \mathbf{B}^{(0)})$;

Iteration counter $i = 0$, maximum iteration number I ;

Error parameters $\xi \in (0, 1)$, $\epsilon \in (0, 1)$.

Output: Optimized $(\mathbf{p}^*, \mathbf{B}^*)$.

1 **Function** *Optimization_of_Power_and_Bandwidth* ($\mathbf{p}, \mathbf{B}, I, \xi, \epsilon$):

2 Compute initial values of auxiliary variables $\boldsymbol{\gamma}, \boldsymbol{\delta}$:

$$\boldsymbol{\gamma}^{(0)} = [\gamma_n^{(0)}]_{n \in \mathcal{N}}, \quad \boldsymbol{\delta}^{(0)} = [\delta_n^{(0)}]_{n \in \mathcal{N}}; \quad (36)$$

$$\text{where } \delta_n^{(0)} = \frac{p_n^{(0)} \rho_n d_n D_n}{r_n(p_n^{(0)}, B_n^{(0)})}, \quad \gamma_n^{(0)} = \frac{\omega_2}{r_n(p_n^{(0)}, B_n^{(0)})}. \quad (37)$$

3 **while** $i \leq I$ and not convergence **do**

4 Solve \mathbb{P}_7 with given $(\boldsymbol{\delta}^{(i)}, \boldsymbol{\gamma}^{(i)})$ based on (56), and obtain a new solution $(\mathbf{p}^{(i+1)}, \mathbf{B}^{(i+1)})$.

5 Compute $\phi(\boldsymbol{\delta}^{(i)}, \boldsymbol{\gamma}^{(i)})$ as follows:

$$\phi(\boldsymbol{\delta}^{(i)}, \boldsymbol{\gamma}^{(i)}) = [\phi_1(\boldsymbol{\delta}^{(i)}), \phi_2(\boldsymbol{\gamma}^{(i)})]^T \in \mathbb{R}^{2N}, \quad (38a)$$

$$\phi_1(\boldsymbol{\delta}^{(i)}) = [\phi_{1,n}(\boldsymbol{\delta}^{(i)})]_{n \in \mathcal{N}}, \quad (38b)$$

$$\phi_2(\boldsymbol{\gamma}^{(i)}) = [\phi_{2,n}(\boldsymbol{\gamma}^{(i)})]_{n \in \mathcal{N}}, \quad (38c)$$

$$\phi_{1,n}(\boldsymbol{\delta}^{(i)}) = -p_n^{(i+1)} \rho_n d_n D_n + \delta_n^{(i)} r_n(p_n^{(i+1)}, B_n^{(i+1)}), \quad (38d)$$

6 $\phi_{2,n}(\boldsymbol{\gamma}^{(i)}) = -\omega_2 + \gamma_n^{(i)} r_n(p_n^{(i+1)}, B_n^{(i+1)})$. (38e)

7 If $\phi(\boldsymbol{\delta}^{(i)}, \boldsymbol{\gamma}^{(i)})$ is approximately a zero vector, then the algorithm terminates, and $(\mathbf{p}^{(i+1)}, \mathbf{B}^{(i+1)})$ is the global optimum $(\mathbf{p}^*, \mathbf{B}^*)$ to \mathbb{P}_4 .

// The algorithm will converge when

$$\phi(\boldsymbol{\delta}^{(i)}, \boldsymbol{\gamma}^{(i)}) = 0 \text{ and the proof is given by Theorem 3.1 in [53]}$$

8 Otherwise, find the smallest integer j satisfying:

$$\begin{aligned} &\| \phi(\boldsymbol{\delta}^{(i)} + \xi^j \boldsymbol{\sigma}_1^{(i)}, \boldsymbol{\gamma}^{(i)} + \xi^j \boldsymbol{\sigma}_2^{(i)}) \|_2 \\ &\leq (1 - \epsilon \xi^j) \| \phi(\boldsymbol{\delta}^{(i)}, \boldsymbol{\gamma}^{(i)}) \|_2, \end{aligned} \quad (39)$$

where $\boldsymbol{\sigma}_1^{(i)}$ and $\boldsymbol{\sigma}_2^{(i)}$ are computed as

$$\boldsymbol{\sigma}_1^{(i)} = -[\phi_1'(\boldsymbol{\delta}^{(i)})]^{-1} \phi_1(\boldsymbol{\delta}^{(i)}), \quad (40)$$

$$\boldsymbol{\sigma}_2^{(i)} = -[\phi_2'(\boldsymbol{\gamma}^{(i)})]^{-1} \phi_2(\boldsymbol{\gamma}^{(i)}). \quad (41)$$

// Here we utilize a modified Newton method, and if j happens to be 0, it becomes a standard Newton Method

9 Update auxiliary variables $(\boldsymbol{\gamma}, \boldsymbol{\delta})$:

$$(\boldsymbol{\delta}^{(i+1)}, \boldsymbol{\gamma}^{(i+1)}) \leftarrow (\boldsymbol{\delta}^{(i)} + \xi^j \boldsymbol{\sigma}_1^{(i)}, \boldsymbol{\gamma}^{(i)} + \xi^j \boldsymbol{\sigma}_2^{(i)}). \quad (42)$$

10 Let $i \leftarrow i + 1$.

11 Utilize the optimized $(\boldsymbol{\delta}^*, \boldsymbol{\gamma}^*)$ to derive the optimal $(\mathbf{p}^*, \mathbf{B}^*)$.

Complementary Slackness:

$$\zeta \cdot \left(\sum_{n=1}^N B_n - B \right) = 0, \quad (45a)$$

$$\eta_n \cdot (r_n^{\min} - r_n(p_n, B_n)) = 0, \quad (45b)$$

$$\nu_n (N_0 B_n S_n^{\min} - p_n g_n) = 0, \quad (45c)$$

$$\iota_n (p_n - p_n^{\max}) = 0. \quad (45d)$$

Primal feasibility: (16a), (16c), (33a), (33b).

Dual feasibility:

$$(46a) : \zeta \geq 0, \quad (46b) : \eta_n \geq 0,$$

$$(46c) : \nu_n \geq 0, \quad (46d) : \iota_n \geq 0.$$

Roadmap: Thereafter, we identify a roadmap to find a set of solution $(\mathbf{p}^*, \mathbf{B}^*)$ by analyzing the Lagrangian multipliers with respect to the corresponding constraints.

Step 1. We first compute \bar{p}_n as a function of (B_n, η_n, ν_n) by setting $\iota_n = 0$ from (44a), which is denoted as:

$$\bar{p}_n(B_n, \eta_n, \nu_n) = \frac{(\gamma_n \delta_n + \eta_n) B_n}{(\gamma_n \rho_n d_n D_n - \nu_n g_n) \ln 2} - \frac{N_0 B_n}{g_n}. \quad (47)$$

Then, we discuss the following two cases to identify the

optimal $p_n^*(B_n, \eta_n, \nu_n)$:

- **Case 1:** $\bar{p}_n(B_n, \eta_n, \nu_n) \leq p_n^{\max}$. In this case, we simply set $\nu_n = 0$ and the optimal $p_n^*(B_n, \eta_n, \nu_n) = \bar{p}_n(B_n, \eta_n, \nu_n)$. All conditions can be satisfied.
- **Case 2:** $\bar{p}_n(B_n, \eta_n, \nu_n) > p_n^{\max}$. Clearly, setting $\nu_n = 0$ is not viable in this scenario, as it would lead to a violation of the primal feasibility condition (16a). Using $\nu_n > 0$ in (45d), it always holds that $p_n^* = p_n^{\max}$.

Summarize both cases and we have the following conclusion:

$$p_n^*(B_n, \eta_n, \nu_n) = \min\{\bar{p}_n(B_n, \eta_n, \nu_n), p_n^{\max}\}. \quad (48)$$

Step 2: Substituting (48) into (45c) and setting $\nu_n = 0$, we could compute SNR S_n as a function of (B_n, η_n) :

$$\bar{S}_n(B_n, \eta_n) = \min\left\{\frac{(\gamma_n \delta_n + \eta_n) g_n}{(\gamma_n \rho_n d_n D_n) N_0 \ln 2} - 1, \frac{p_n^{\max} g_n}{N_0 B_n}\right\}. \quad (49)$$

Then, we discuss the following two cases:

- **Case 1:** $\bar{S}_n(B_n, \eta_n) \geq S_n^{\min}$. Similarly, we could set $\nu_n = 0$ and the optimal $S_n^* = \bar{S}_n(B_n, \eta_n)$.
- **Case 2:** $\bar{S}_n(B_n, \eta_n) < S_n^{\min}$. Setting $\nu_n = 0$ in this case will violate primal feasibility (33b). Thereafter, we substitute $\nu_n > 0$ in (45c), it always holds that $S_n^* = S_n^{\min}$ and we can derive that $\bar{\nu}_n(B_n, \eta_n) = \frac{\gamma_n \rho_n d_n}{g_n} - \frac{(\gamma_n \delta_n + \eta_n) g_n}{(\min\{S_n^{\min}, \frac{p_n^{\max} g_n}{N_0 B_n}\} + 1) N_0 \ln 2}$.

Summarize both cases, and we have the following conclusion:

$$S_n^*(B_n, \eta_n) = \max\{\bar{S}_n(B_n, \eta_n), S_n^{\min}\}. \quad (50)$$

Combining (45c) and (50), we can also derive the optimal $\nu_n^*(B_n, \eta_n)$ as follows:

$$\nu_n^*(B_n, \eta_n) = \begin{cases} 0 & \text{if } \bar{S}_n(B_n, \eta_n) \geq S_n^{\min}, \\ \bar{\nu}_n(B_n, \eta_n) & \text{otherwise.} \end{cases} \quad (51)$$

Step 3. Then, we analyze the multiplier η . Substituting (50) into (45b), we could derive $\bar{r}_n(B_n)$ by setting $\eta_n = 0$:

$$\bar{r}_n(B_n) = B_n \log_2(1 + S_n^*(B_n, \eta_n) |_{\eta_n=0}), \quad (52)$$

We discuss the following two cases:

- **Case 1:** $\bar{r}_n(B_n) \geq r_n^{\min}$. We set $\eta_n = 0$ and the optimal $r_n^*(B_n) = \bar{r}_n(B_n)$.
- **Case 2:** $\bar{r}_n(B_n) < r_n^{\min}$. Setting $\eta_n = 0$ will violate primal feasibility (33a). Using $\eta_n > 0$ in (45b), it always holds that $r_n^*(B_n, \eta_n) = r_n^{\min}$. Solve the above equation and obtain the optimal solution denoted as $\bar{\eta}_n(B_n)$.

Summarize both cases and we have the following conclusion:

$$\eta_n^*(B_n) = \begin{cases} 0 & \text{if } \bar{r}_n(B_n) \geq r_n^{\min}, \\ \bar{\eta}_n(B_n) & \text{otherwise.} \end{cases} \quad (53)$$

Step 4. Substituting (48), (51), (53) into stationarity (44b), the following equation could be derived:

$$-(\gamma_n \delta_n + \eta_n^*(B_n)) \log_2(1 + S_n^*(B_n)) + \frac{(\gamma_n \delta_n + \eta_n^*(B_n)) S_n^*(B_n)}{(1 + S_n^*(B_n)) \ln 2} + \zeta + \nu_n^*(B_n) N_0 S_n^{\min} = 0. \quad (54)$$

From (54) we could derive the solution denoted as $\bar{B}_n(\zeta)$. We calculate $\sum_{n=1}^N \bar{B}_n(0)$ with $\zeta = 0$, and then considering:

- **Case 1:** $\sum_{n=1}^N \bar{B}_n(0) \leq B_{\text{total}}$. Set $\zeta = 0$ and the optimal $B_n^* = B_n(0)$.
- **Case 2:** $\sum_{n=1}^N \bar{B}_n(0) > B_{\text{total}}$. Using $\zeta > 0$ in (45a) and we have $\sum_{n=1}^N \bar{B}_n(\zeta) = B_{\text{total}}$. A bisection method could be applied to solve the equation and find the solution $\bar{\zeta}$.

Summarize both cases and we have:

$$\zeta^* = \begin{cases} 0 & \text{if } \sum_{n=1}^N \bar{B}_n(0) \leq B_{\text{total}}, \\ \bar{\zeta} & \text{otherwise.} \end{cases} \quad (55)$$

Until now, we have analyzed all the variables, and the optimal solution $(\mathbf{p}^*, \mathbf{B}^*)$ could be expressed as:

$$\begin{cases} B_n^* = B_n(\zeta^*), \\ p_n^* = \min\{\bar{p}_n(B_n^*, \eta_n^*, \nu_n^*), p_n^{\max}\}. \end{cases} \quad (56)$$

C. Resource Allocation Algorithm

Based on the analysis in Sections V-A and V-B, we have solved Problems \mathbb{P}_3 and \mathbb{P}_4 respectively. Thereafter, we give the resource allocation algorithm, as shown in Algorithm 3 below, to iteratively solve \mathbb{P}_3 and \mathbb{P}_4 until convergence.

Algorithm 3: Resource Allocation Algorithm

Input: Initial solution $sol^{(0)} = (\mathbf{p}^{(0)}, \mathbf{B}^{(0)}, \mathbf{f}^{(0)}, \mathbf{h}^{(0)}, \boldsymbol{\rho}^{(0)})$;
Maximum iteration number K ;
Error parameter $\epsilon \in (0, 1)$.
Output: Optimal solution $sol^* = (\mathbf{p}^*, \mathbf{B}^*, \mathbf{f}^*, \mathbf{h}^*, \boldsymbol{\rho}^*)$.

- 1 **Function** *Joint_Optimization* ($sol^{(0)}, K, \epsilon$):
- 2 Set iteration counter $k = 0$.
- 3 **while** $k \leq K$ and not convergence **do**
- 4 Solve \mathbb{P}_3 through (32) on page 7 with $(\mathbf{p}^{(k)}, \mathbf{B}^{(k)})$, and obtain $(\mathbf{f}^{(k+1)}, \mathbf{h}^{(k+1)}, \boldsymbol{\rho}^{(k+1)}, \mathcal{T}^{(k+1)})$.
- 5 Solve \mathbb{P}_4 by calling Algorithm 2 on page 8 with $(\mathbf{f}^{(k+1)}, \mathbf{h}^{(k+1)}, \boldsymbol{\rho}^{(k+1)}, \mathcal{T}^{(k+1)})$ to obtain $(\mathbf{p}^{(k+1)}, \mathbf{B}^{(k+1)})$.
- 6 Update the solution:
 $sol^{(k+1)} \leftarrow (\mathbf{p}^{(k+1)}, \mathbf{B}^{(k+1)}, \mathbf{f}^{(k+1)}, \mathbf{h}^{(k+1)}, \boldsymbol{\rho}^{(k+1)})$.
- 7 If $|sol^{(k+1)} - sol^{(k)}| \leq \epsilon$, the algorithm terminates.
- 8 Let $k \leftarrow k + 1$
- 9
- 10 Return the optimal $sol^* = (\mathbf{p}^*, \mathbf{B}^*, \mathbf{f}^*, \mathbf{h}^*, \boldsymbol{\rho}^*)$

VI. TIME COMPLEXITY, SOLUTION QUALITY AND CONVERGENCE ANALYSIS

This section offers a detailed analysis of Algorithm 3, focusing on its time complexity, the quality of solutions, and its convergence

A. Time Complexity

The bulk of the computational load in Algorithm 3 resides in steps 4 and 5. Step 4 involves using the bisection method to solve \mathbb{P}_3 and to compute the parameters $\mathbf{f}, \mathbf{h}, \boldsymbol{\rho}$ and \mathcal{T} . Given that the bisection method's complexity is independent of N and hinges only on the desired precision, step 3 incurs a complexity of $\mathcal{O}(4N)$. In step 5, Algorithm 2 iteratively solves \mathbb{P}_7 and updates auxiliary variables until the convergence, where the maximum iteration number is I . The computation of \mathbf{B} and \mathbf{p} , along with the updates to $\boldsymbol{\delta}$ and $\boldsymbol{\gamma}$, takes $\mathcal{O}(4N)$. Additional steps 5, 7, and 8 in Algorithm 2 incur complexities of $\mathcal{O}(2N)$, $\mathcal{O}((j+1)N)$, and $\mathcal{O}(2N)$, respectively. Considering a maximum iteration count of I , the overall complexity for Algorithm 2 is thus approximated as $\mathcal{O}(I(j+9)N)$. Accounting for the fact that Algorithm 3 iteratively solves \mathbb{P}_3 and \mathbb{P}_4 with a maximum of K iterations, we deduce that the total time complexity is $\mathcal{O}(K(Ij+9I+4)N)$.

B. Solution Quality

The proposed Algorithm 3 iteratively optimizes two variable sets, $[\mathbf{f}, \mathbf{h}, \boldsymbol{\rho}, \mathcal{T}]$ and $[\mathbf{p}, \mathbf{B}]$, by solving problems \mathbb{P}_3 and \mathbb{P}_4 alternately. For \mathbb{P}_3 , Lemma 2 demonstrates that the KKT conditions are both necessary and sufficient for optimality due to the problem's convexity. This affirmation means that a globally optimal solution can be reliably obtained. Moreover, Algorithm 2 aims to solve \mathbb{P}_4 , and based on Theorem 1, \mathbb{P}_7 is proven to have the same globally optimal solution as \mathbb{P}_4 . Therefore, although the alternating optimization approach does not always assure a local or global optimum for \mathbb{P}_1 , the global optimality of the subproblems can be secured. The precision parameter ϵ in Algorithm 3 guarantees the solution's convergence to a desired level of accuracy.

C. Convergence

Convergence begins with the resolution of \mathbb{P}_3 using the KKT conditions within Algorithm 3. Given the convex nature of \mathbb{P}_3 when \mathbf{p} and \mathbf{B} are fixed, we ensure both the optimality and convergence, as dictated by Lemma 2.

The convergence of \mathbb{P}_4 solved by Algorithm 2 merits further discussion. Let $\mathbf{v} = (\boldsymbol{\delta}, \boldsymbol{\gamma})$ for brevity. Drawing on Theorem 3.2 in [53], convergence is assured if:

- 1) The function $\phi(\mathbf{v})$ is differentiable and meets the Lipschitz condition within the solution domain Ω .
- 2) A constant $L > 0$ exists, such that $|\phi'(\mathbf{v}_1) - \phi'(\mathbf{v}_2)| \leq L|\mathbf{v}_1 - \mathbf{v}_2|$ for all $\mathbf{v}_1, \mathbf{v}_2 \in \Omega$.
- 3) A constant $M > 0$ can be found for which $|\phi'(\mathbf{v})| \leq M$ holds true for all $\mathbf{v} \in \Omega$.

Under these stipulations, the modified Newton method used in Algorithm 2 converges linearly to the optimal solution \mathbf{v}^* from any starting point $\mathbf{v}_0 \in \Omega$, and this convergence becomes quadratic in the vicinity of \mathbf{v}^* . The function $\phi(\mathbf{v})$ is linear and readily satisfies conditions 1)-3), as shown in [53]. With \mathbf{v} given, the KKT conditions are again employed to determine the optimal $(\mathbf{p}^*, \mathbf{B}^*)$. This analysis substantiates the convergence of Algorithm 2.

VII. SIMULATION

This section first introduces the adopted SemCom models, accuracy functions and parameter settings. Then, experiments are conducted to demonstrate our method's effectiveness.

A. Semantic Communication Model

We utilize a deep joint source and channel coding (JSCC) model, as outlined in [38], for our image semantic communication model. The deep JSCC architecture has been widely applied in semantic communication studies [57]–[59]. The model functions as an end-to-end autoencoder, consisting of two convolutional neural networks (CNNs) that serve as the encoder and decoder. These components are jointly trained with a non-trainable layer in the middle that simulates the noisy communication channel.

In particular, the encoder CNN consists of five convolutional layers followed by parametric ReLU (PReLU) activation functions and a normalization layer. This architecture extracts

and combines image features from the original image to form the channel input samples for transmission. Conversely, the decoder CNN processes the received coded signal (possibly noised) through a series of transposed convolutional layers with non-linear activation functions, using these features to reconstruct an estimated image.

B. Performance Function Fitting

We evaluate the PSNR performance of the adopted model on the CIFAR-10 dataset, which is aligned with the choice of deep JSCC [38]. Specifically, CIFAR-10 consists of color images with a 32×32 pixels resolution.

Performance function. The PSNR performance function $P(\rho_n, S_n)$ for each user n has two variables: compression rate ρ_n and SNR S_n . A higher ρ_n improves accuracy by minimizing information loss in compression, while a higher SNR ensures better semantic content quality and reliability. We employ curve-fitting techniques to develop function $P(\rho_n, S_n)$, and the specific expression is adapted from logarithmic models in previous works [60], reflecting diminishing returns:

$$P(\rho_n, S_n) = a \ln(c^\rho \rho_n + c^s S_n + b), \quad (57)$$

where a, b, c^ρ and c^s are coefficients decided by fitting data.

Given the multidimensional nature of $P(\rho_n, S_n)$, we simplify visual interpretation by transforming it into a two-dimensional plot. Let ρ_n^{\max} (resp., S_n^{\max}) be the maximum ρ_n (resp., S_n) from the dataset. Upon introducing the notation $l = c^\rho \rho_n^{\max} + c^s S_n^{\max}$, we proceed to assign $\frac{c^\rho}{l} \rho_n + \frac{c^s}{l} S_n$ as the x -axis coordinate, and plot $a \ln(lx + b)$ as the y -axis coordinate. This choice is motivated by the fact that $P(\rho_n, S_n) = a \ln(c^\rho \rho_n + c^s S_n + b) = a \ln(lx + b)$, thus allowing for a direct representation of the function. Following the mentioned transformation, the x -coordinate of each data point now falls within the range of 0 and 1.

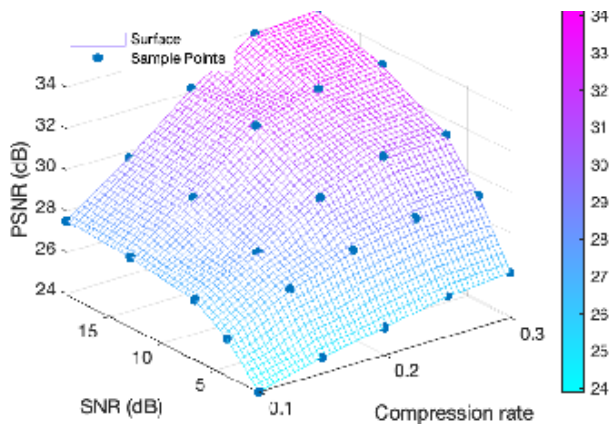
Modelling results. We use the linear method in *scatteredInterpolant* function of Matlab for interpolation. Compared with other interpolation methods (e.g., “nearest” and “natural”), linear interpolation provides smooth transitions between data points without excessive oscillations or discontinuities, and the overall data trend is also maintained well. In addition, we also employ a 5-fold cross-validation to ensure the interpolation accuracy. The entire procedure is repeated ten times and the average mean absolute error (MAE) errors on all folds are 0.4381. The interpolation and function fitting performance and the fitted function are shown in Fig. 2. The expression for the fitted function in Fig. 2(b) is further stated as follows:

$$P(x) = 18.67 \ln(3.35x + 5.11), \text{ for } x = 1.52\rho + 0.03S. \quad (58)$$

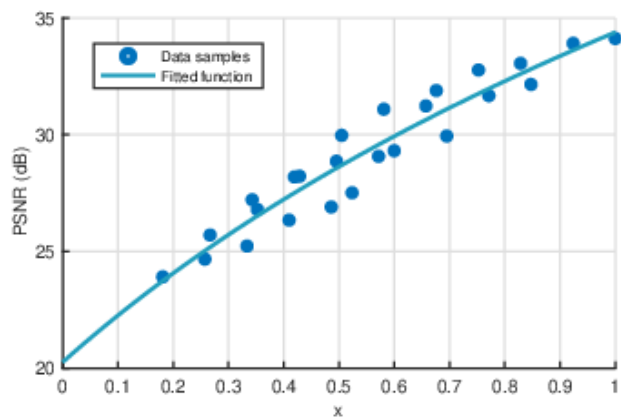
C. Parameter Settings

Our experiments employ a foundational set of parameters as defaults, primarily adapted from [42]. Table II summarizes the overall system settings. The channel model is devised for urban landscapes, encompassing a path loss calculated by $128.1 + 37.6 \log(\text{distance})$ with an 8 dB standard deviation. Gaussian noise power spectral density $N_0 = -174$ dBm/Hz represents thermal noise at 20°C.

Users are randomly dispersed within a circular area with a 500-meter diameter centered on the base station. The system



(a) Interplotted surface for CIFAR-10.



(b) Fitted function for CIFAR-10.

Fig. 2: Interplotted surfaces and fitted results for CIFAR-10. Specifically, each data point (i.e., different SNR and compression rate) was run ten times, and the average accuracy was taken to reduce experimental error.

contains 50 users and a total bandwidth of 20 MHz. The effective switched capacitance (κ , 10^{-28}) and the sample size in a batch (D_n , 32) are preset. CPU cycle requirements (c_{1n}) and (c_{2n}) randomly range from $[1, 3] \times 10^6$ and $[3, 5] \times 10^6$, respectively. The data size (d_n) is 1 Mbits. The maximum transmission power (p_n^{\max}) and device computing frequency (f_n^{\max}) are 20 dBm and 1 GHz. The maximum allocated frequency to device n at BS (h_n^{\max}) is 5 GHz. The PSNR threshold P_n^{\min} is initialized at 25 dB. The semantic compression ratio ρ is between (ρ_n^{\min} , 0.1) and (ρ_n^{\max} , 0.3).

TABLE II: System Parameter Settings

Parameter	Value
The path loss model	$128.1 + 37.6 \log(d)$
The standard deviation of shadow fading	8 dB
Noise power spectral density N_0	-174 dBm/Hz
The number of users N	50
Total Bandwidth B	20 MHz
Effective switched capacitance κ	10^{-28}
The number of samples D_n	32
CPU cycles on each device c_{1n}	$[1, 3] \times 10^6$
CPU cycles on the BS c_{2n}	$[3, 5] \times 10^6$
The uploaded data size d_n	1 Mbits
Max. uplink transmission power p_n^{\max}	20 dBm
Max. device computing frequency f_n^{\max}	1 GHz
Max. BS frequency allocated to device h_n^{\max}	5 GHz
The PSNR threshold P_n^{\min}	25 dB
Min. semantic compression ratio ρ_n^{\min}	0.1
Max. semantic compression ratio ρ_n^{\max}	0.3

D. Comparison of Different Baselines

We first compare our proposed Algorithm 3 with the following 4 baselines:

- (i) **Random Allocation:** For each device n , the quantities p_n, f_n, h_n, ρ_n take random values from $[0, p_n^{\max}]$, $[0, f_n^{\max}]$, $[0, h_n^{\max}]$, $[\rho_n^{\min}, \rho_n^{\max}]$ respectively. A truncated normal distribution is employed for this purpose, centered at the range's midpoint and with a standard deviation set to one-tenth of the range width. Besides, B_n is selected from $[\frac{B_{\text{total}}}{1.25N}, \frac{B_{\text{total}}}{0.8N}]$ and the sum of B_n is equal to B_{total} .

- (ii) **Average Allocation:** Here we set each B_n as $\frac{B_{\text{total}}}{N}$, and p_n, f_n, h_n, ρ_n as $\frac{p_n^{\max}}{2}, \frac{f_n^{\max}}{2}, \frac{h_n^{\max}}{2}, \frac{\rho_n^{\max} + \rho_n^{\min}}{2}$ respectively to evenly distribute resources.
- (iii) **Optimize p, B only:** Here we fix each f_n, h_n and ρ_n as the default settings in Average Allocation. Then, we optimize p_n and B_n of each device n .
- (iv) **Optimize f, h, ρ only:** Each p_n and B_n are fixed as in Average Allocation, and we only optimize f_n, h_n and ρ_n of each device n .

Then, we compare the performance between our proposed method and baselines under varying resource conditions. To reduce the interference of randomness, we choose data points uniformly and run each experiment 100 times to take the average value as the final result.

Total Bandwidth. Here we vary the total available bandwidth B_{total} from 1 MHz to 20 MHz. Figs. 3(a),(b), and (c) demonstrate the total time completion T , energy consumption E , and weighted sum $\omega_1 T + \omega_2 E$ with respect to B_{total} . Higher total bandwidth means more available communication resources so that the general decreasing trend can be observed in the curves of each figure.

Specifically, in Fig. 3(a), we can see our proposed method stays optimal under different B_{total} . Besides, "Optimize p, B only" outperforms "Optimize f, h, ρ only" as B_{total} increases. We analyze that it is because "Optimize p, B only" could bring better communication optimization in the case of abundant bandwidth resources. Fig. 3(b) presents the overall energy consumption. The computation in training incurs more energy overhead compared to transmission. Hence, our proposed method and "Optimize f, h, ρ only" could obtain much better performance on energy optimization. The performance of our method on E is also better than other benchmarks. In Fig. 3(c), our method outperforms all the baselines under different B_{total} .

Maximum Transmission Power. We vary the maximum transmission power p_n^{\max} from 4 dBm to 20 dBm, and show the experimental results in Figs. 4(a),(b) and (c). Higher p_n^{\max} indicates lower limits on the energy consumption E ; hence, the algorithm could utilize higher transmission power to optimize time consumption T .

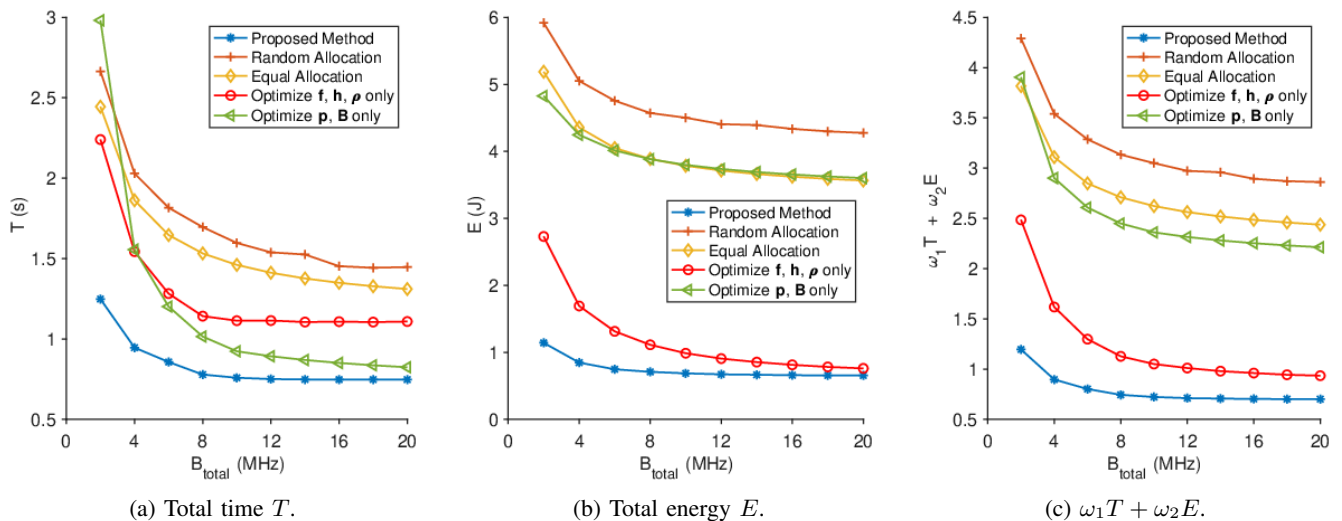


Fig. 3: Time, energy, and their weighted sum under different total bandwidth B_{total} .

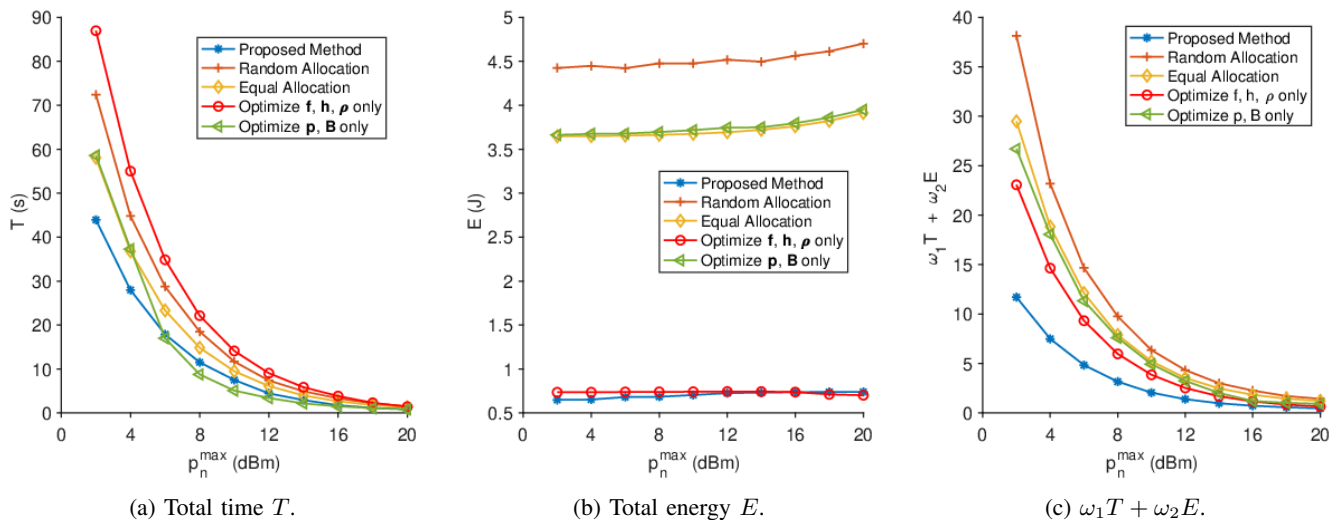


Fig. 4: Time, energy, and their weighted sum under different maximum transmission power p_n^{\max} .

In Fig. 4(a), all curves show a downward trend on T , which is consistent with our analysis above. It is worth noting that although “Optimize p, B only” sometimes could achieve smaller T than ours, the gap is much smaller than that of E . We can observe a moderate rise of E in Fig. 4(b). This is because as the range of p_n^{\max} expands, more optimal solutions p could be chosen to bring about better joint optimization by sacrificing energy optimization to some extent. Finally, in Fig. 4(c), the proposed method still has the best joint optimization performance, proving the superiority of our method.

Maximum Device Computation Frequency. We vary the maximum CPU frequencies f_n^{\max} from 0.1 GHz to 1 GHz and compare T and E in Fig. 5(a) and Fig. 5(b). Intuitively, higher CPU frequency means shorter computation latency but higher energy consumption. Thus, there is a downward trend for curves in Fig. 5(a) and vice versa in Fig. 5(b), respectively. It is also notable that our proposed method and “Optimize f, ρ only” will enter a stationary phase as the f_n^{\max} continuously increase. This is because the optimal frequencies have already

been found. In Fig. 5(c), it is evident that our proposed method always remains the best.

The above experiments demonstrate our proposed method’s superiority over benchmarks across various resource scenarios.

E. Weight Parameters

Here, we study how values of weight parameters influence our algorithm’s performance. In our problem, there are two weight parameters ω_1 and ω_2 , and the sum of them equals 1. If the system is more sensitive to latency, the parameter ω_1 for T should be set as a larger value. Then, if the system has higher requirements for low energy consumption, ω_2 for E should be raised accordingly.

We set the parameter ω_1 within the range of 0.1 to 0.9, while ω_2 is configured as $1 - \omega_1$. The experimental result is reported in Figs. 6(a) and (b). In Fig. 6(a), we can see as ω_1 increases, the time consumption continues to decrease. This is due to a larger ω_1 could motivate our algorithm to allocate more resources to the optimization of time. Similarly, a decrease

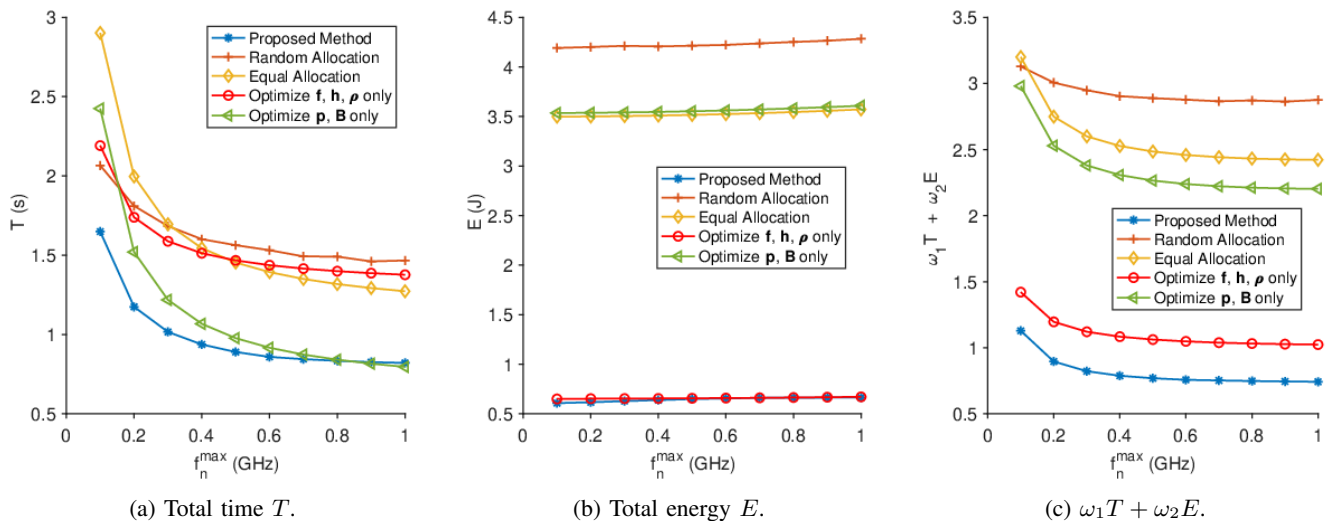


Fig. 5: Time, energy, and their weighted sum under different maximum frequency f_n^{\max} .

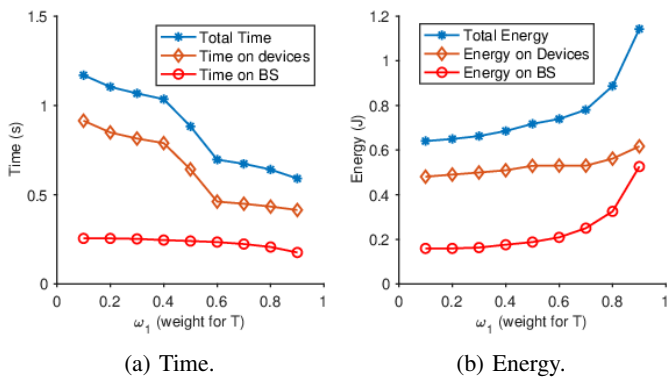


Fig. 6: Time and energy under different weight parameters ω_1 .

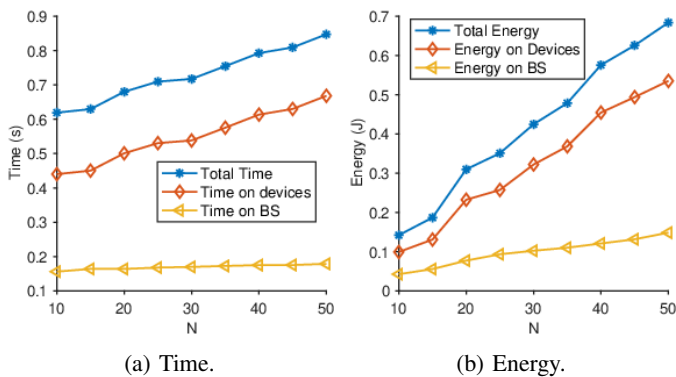


Fig. 7: Time and energy under different numbers of users N .

in ω_2 represents less emphasis on energy optimization, so the total energy consumption E in Fig. 6(b) increases. In addition to this, we find that the users' overhead is greater than that of the BS. This is due to the fact that our algorithm optimizes the computational overhead more efficiently, making the uplink transmission, which is the responsibility of the user, the main source of overhead.

F. Number of Users

Next, we explore the effect of the total number of mobile devices N on optimization performance. Intuitively, when the total available resources are fixed, a larger number of N could increase the overall consumption within the system as more communications and computations are required.

Specifically, we vary the number of mobile devices N from 10 to 50, and the corresponding results are reported in Figs. 7(a) and (b). In Fig. 7(a), we could observe an overall increasing trend in time, especially on devices. This is because the total bandwidth B_{total} is fixed; as the number of users N increases, the average bandwidth allocated per user n decreases, leading to longer transmission times. In Fig. 7(b), there is a sharper increase in energy consumption due to longer transmission times consuming more energy.

G. SemCom performance Analysis

In this section, we vary minimum PSNR value requirements P_n^{\min} on the system and observe how the model performance and consumption will be affected. Intuitively, higher P_n^{\min} leads to better performance of the SemCom but also sacrifices somewhat the optimization of overall consumption.

We increase P_n^{\min} from 20 dB to 30 dB to compare the PSNR values and consumption metrics. Specifically, Fig. 8(a) demonstrates that the average of PSNR values among all devices increases as P_n^{\min} grows. The shallow blue-filled areas "Range" show the minimum and maximum PSNR observed in all devices. Meanwhile, Fig. 8(b) illustrates that energy and time consumption also have increasing trends. This correlation is expected: increasing P_n^{\min} leads our algorithm to prioritize model performance for each mobile device, which is often at the expense of other optimizations like higher power usage, increased compression rate, or reduced bandwidth.

We further compare our model's performance under different training settings (i.e., performance requirement P_n^{\min}) with that of the typical JPEG technique, and the result is as shown in Fig. 9. Particularly, Fig. 9(a) presents an original

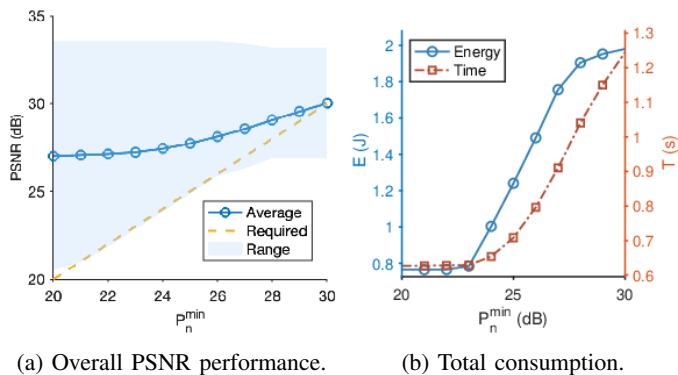


Fig. 8: Comparison of PSNR values and overall consumption under different P_n^{\min}

example image from CIFAR-10. Figs. 9(b) and (c) provide visualizations of the reconstructed images by Semcom models under different training settings. Fig. 9(d) is the generated image by JPEG. For fairness, the tested SNR values are all set at 10 dB. We can see that even under a challenging training condition (SNR=4 dB and $\rho = 0.1$, i.e., $P_n^{\min}=25.70$ dB), our model still achieves a PSNR of 25.67 dB, comparable to that of JPEG (26.13 dB). When the training condition is improved into (SNR=13 dB and $\rho = 0.1$, i.e., $P_n^{\min}=26.79$ dB), our PSNR value achieves 26.95 dB, outperforming JPEG. This is because JPEG traditionally compresses images based on the pixel level and cannot resist noise effectively. In contrast, our semantic communication model accounts for channel noise during training and has learned image restoration techniques to mitigate the effects of noise.

H. Scalability on High-Resolution Images

Here we further test the scalability of the trained model when dealing with an image of higher resolution (512×768). Particularly, the selected image did not appear in the training dataset (zero-shot) and is more complicated than the training ones (32×32). Figs. 10(a)-(d) shows the original image and our experimental results. From Fig. 10(b), we can see our model could achieve a PSNR value of 25.75 dB (SNR = 13dB, $\rho = 0.1$), only slightly lower than that of JPEG (25.89 dB) in Fig. 10(d). When under a challenging condition (SNR=4 dB, $\rho = 0.1$), the model could still achieve a PSNR value of 23.21 dB, as shown in Fig. 10(c). Thereafter, we believe that if sufficiently trained on more complex datasets, the semantic communication model can achieve performance comparable to or even beat JPEG.

VIII. DISCUSSION & CONCLUSION

Generalizability: Our current SemCom model is evaluated under AWGN channels for analytical simplicity [16], [28], [47], [47], [61]. However, it is inherently adaptable to other channel conditions. For instance, the deep JSCC model can be extended to fading channels, such as Rayleigh and Rician, by incorporating non-trainable differentiable layers, as demonstrated in [16], [38], [62]. Additionally, our resource allocation

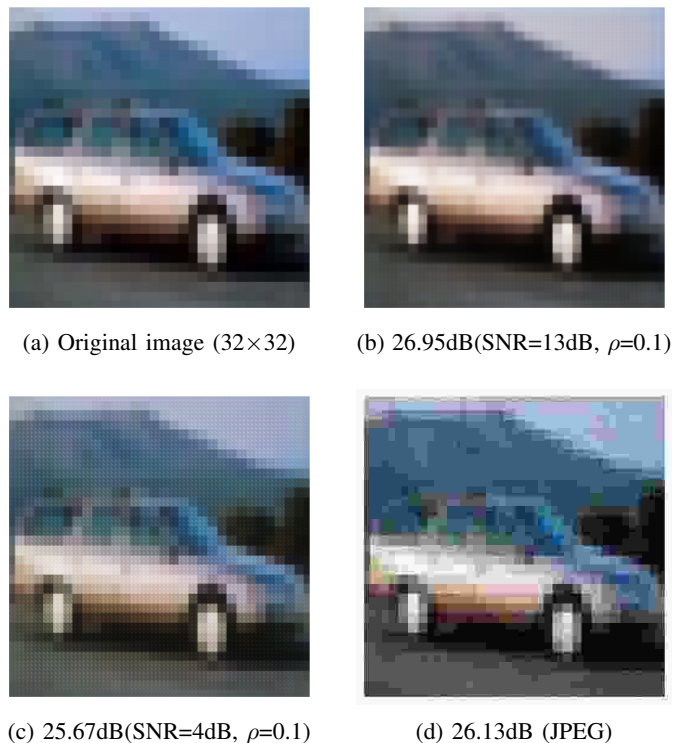


Fig. 9: PSNR values of reconstructed images by our SemCom model and JPEG under different settings, e.g., (SNR=13dB, $\rho=0.1$) denotes the model trained with an SNR=13 dB and a compression rate=0.1.

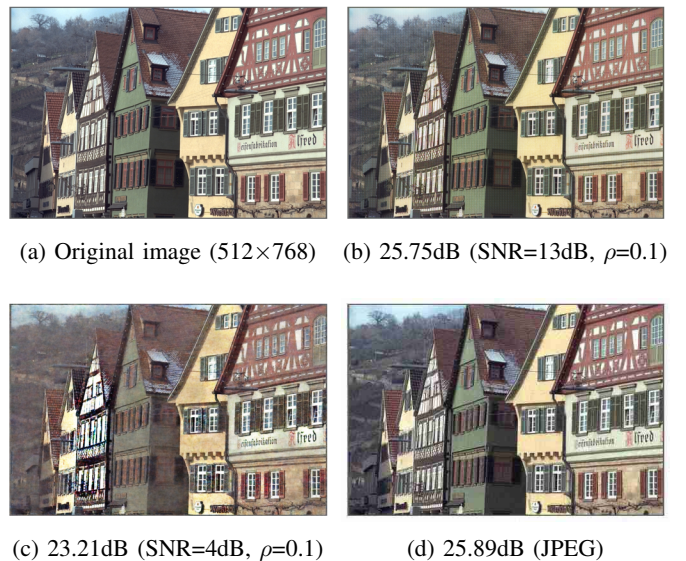


Fig. 10: PSNR values of reconstructed images by our SemCom model and JPEG under different settings.

algorithm is designed to be robust across different channel models, as it does not rely on specific channel parameters as optimization variables. This ensures the algorithm's applicability in diverse real-world communication environments, making it suitable for various use cases.

Deep Reinforcement Learning (DRL) Approaches. In this

work, we rely on a centralized decision-making process and archive the “order optimality (i.e., $\mathcal{O}(N)$)” in time complexity for efficiency. Another promising solution to our problem is DRL. DRL methods have demonstrated significant promise in addressing complex resource allocation challenges within distributed systems [63]–[67]. These approaches leverage the ability of RL to make sequential decisions while incorporating the power of deep neural networks to process high-dimensional state and action spaces. DRL is particularly well-suited for solving non-convex optimization problems [66], [67], especially in time-sensitive scenarios. In future work, we aim to explore DRL-based approaches to the system model, seeking the feasibility to further enhance the scalability and efficiency of resource allocation strategies.

Conclusion. In this paper, we introduce a distributed image semantic communication system where the local devices and base station train the SemCom model collaboratively. We also study how to optimize transmission power, bandwidth, computing frequency and compression rate to minimize a weighted sum of time and energy consumption while guaranteeing the model performance. A resource allocation algorithm is further proposed to solve the joint optimization problem. Time complexity, solution quality and convergence are also analyzed. In experiments, we first compare our method with benchmarks under different resource conditions and then investigate the influence of weight parameters, number of users, and accuracy requirements. The experimental results demonstrate the effectiveness and superiority of our method.

REFERENCES

- [1] Y. Wang, Z. Gao, D. Zheng, S. Chen, D. Gunduz, and H. V. Poor, “Transformer-empowered 6G intelligent networks: From massive MIMO processing to semantic communication,” *IEEE Wireless Communications*, 2022.
- [2] L. U. Khan, W. Saad, D. Niyato, Z. Han, and C. S. Hong, “Digital-twin-enabled 6G: Vision, architectural trends, and future directions,” *IEEE Communications Magazine*, vol. 60, no. 1, pp. 74–80, 2022.
- [3] Z. Zhang, X. Lin, G. Xue, Y. Zhang, and K. S. Chan, “Joint optimization of task offloading and resource allocation in tactical edge networks,” in *MILCOM 2024-2024 IEEE Military Communications Conference (MILCOM)*. IEEE, 2024, pp. 703–708.
- [4] Y. Wang, Z. Su, S. Guo, M. Dai, T. H. Luan, and Y. Liu, “A survey on digital twins: architecture, enabling technologies, security and privacy, and future prospects,” *IEEE Internet of Things Journal*, 2023.
- [5] K. Qu, W. Zhuang, Q. Ye, W. Wu, and X. Shen, “Model-assisted learning for adaptive cooperative perception of connected autonomous vehicles,” *IEEE Transactions on Wireless Communications*, 2024.
- [6] Q. Ye, W. Shi, K. Qu, H. He, W. Zhuang, and X. Shen, “Joint RAN slicing and computation offloading for autonomous vehicular networks: A learning-assisted hierarchical approach,” *IEEE Open Journal of Vehicular Technology*, vol. 2, pp. 272–288, 2021.
- [7] F. Wang, Z. Li, and J. Han, “Continuous user authentication by contactless wireless sensing,” *IEEE Internet of Things Journal*, vol. 6, no. 5, pp. 8323–8331, 2019.
- [8] Y. Lin, H. Du, D. Niyato, J. Nie, J. Zhang, Y. Cheng, and Z. Yang, “Blockchain-aided secure semantic communication for AI-generated content in metaverse,” *IEEE Open Journal of the Computer Society*, vol. 4, pp. 72–83, 2023.
- [9] J. Park, J. Choi, S.-L. Kim, and M. Bennis, “Enabling the wireless metaverse via semantic multiverse communication,” in *2023 20th Annual IEEE International Conference on Sensing, Communication, and Networking (SECON)*. IEEE, 2023, pp. 85–90.
- [10] Z. Yang, P. Nguyen, H. Jin, and K. Nahrstedt, “MIRAS: Model-based reinforcement learning for microservice resource allocation over scientific workflows,” in *2019 IEEE 39th International Conference on Distributed Computing Systems (ICDCS)*. IEEE, 2019, pp. 122–132.
- [11] S. Pala, M. Katwe, K. Singh, B. Clerckx, and C.-P. Li, “Spectral-efficient RIS-aided RSMA URLLC: Toward mobile broadband reliable low latency communication (mBRLLC),” *IEEE Transactions on Wireless Communications*, 2023.
- [12] B. Hu, Y. Gao, W. Zhang, D. Jia, and H. Liu, “Computation offloading and resource allocation in IoT-based mobile edge computing systems,” in *2023 IEEE International Conference on Smart Internet of Things (SmartIoT)*. IEEE, 2023, pp. 119–123.
- [13] C. E. Shannon and W. Weaver, *The Mathematical Theory of Communication*. University of Illinois Press, 1949.
- [14] Z. Qin, X. Tao, J. Lu, W. Tong, and G. Y. Li, “Semantic communications: Principles and challenges,” *arXiv preprint arXiv:2201.01389*, 2021.
- [15] H. Zhang, S. Shao, M. Tao, X. Bi, and K. B. Letaief, “Deep learning-enabled semantic communication systems with task-unaware transmitter and dynamic data,” *IEEE Journal on Selected Areas in Communications*, vol. 41, no. 1, pp. 170–185, 2022.
- [16] H. Xie, Z. Qin, G. Y. Li, and B.-H. Juang, “Deep learning enabled semantic communication systems,” *IEEE Transactions on Signal Processing*, vol. 69, pp. 2663–2675, 2021.
- [17] Y. Liu, S. Jiang, Y. Zhang, K. Cao, L. Zhou, B.-C. Seet, H. Zhao, and J. Wei, “Extended context-based semantic communication system for text transmission,” *Digital Communications and Networks*, 2022.
- [18] E. Kutay and A. Yener, “Semantic text compression for classification,” in *2023 IEEE International Conference on Communications Workshops (ICC Workshops)*. IEEE, 2023, pp. 1368–1373.
- [19] X. Peng, Z. Qin, D. Huang, X. Tao, J. Lu, G. Liu, and C. Pan, “A robust deep learning enabled semantic communication system for text,” in *IEEE Global Communications Conference (GLOBECOM)*. IEEE, 2022, pp. 2704–2709.
- [20] D. Huang, X. Tao, F. Gao, and J. Lu, “Deep learning-based image semantic coding for semantic communications,” in *2021 IEEE Global Communications Conference (GLOBECOM)*. IEEE, 2021, pp. 1–6.
- [21] M. U. Lokumarambage, V. S. S. Gowrisetty, H. Rezaei, T. Sivalingam, N. Rajatheva, and A. Fernando, “Wireless end-to-end image transmission system using semantic communications,” *IEEE Access*, 2023.
- [22] E. Grassucci, C. Marinoni, A. Rodriguez, and D. Communiello, “Diffusion models for audio semantic communication,” in *ICASSP 2024-2024 IEEE International Conference on Acoustics, Speech and Signal Processing (ICASSP)*. IEEE, 2024, pp. 13 136–13 140.
- [23] P. Jiang, C.-K. Wen, S. Jin, and G. Y. Li, “Wireless semantic communications for video conferencing,” *IEEE Journal on Selected Areas in Communications*, vol. 41, no. 1, pp. 230–244, 2022.
- [24] A. Vaswani, N. Shazeer, N. Parmar, J. Uszkoreit, L. Jones, A. N. Gomez, Ł. Kaiser, and I. Polosukhin, “Attention is all you need,” *Advances in neural information processing systems*, vol. 30, 2017.
- [25] K. Weiss, T. M. Khoshgoftaar, and D. Wang, “A survey of transfer learning,” *Journal of Big Data*, vol. 3, no. 1, pp. 1–40, 2016.
- [26] Z. Dai, Z. Yang, Y. Yang, J. Carbonell, Q. V. Le, and R. Salakhutdinov, “Transformer-xl: Attentive language models beyond a fixed-length context,” *arXiv preprint arXiv:1901.02860*, 2019.
- [27] N. Reimers, “Sentence-bert: Sentence embeddings using siamese bert-networks,” *arXiv preprint arXiv:1908.10084*, 2019.
- [28] Z. Weng and Z. Qin, “Semantic communication systems for speech transmission,” *IEEE Journal on Selected Areas in Communications*, vol. 39, no. 8, pp. 2434–2444, 2021.
- [29] L. Yan, Z. Qin, R. Zhang, Y. Li, and G. Y. Li, “Resource allocation for text semantic communications,” *IEEE Wireless Communications Letters*, vol. 11, no. 7, pp. 1394–1398, 2022.
- [30] —, “QoE-aware resource allocation for semantic communication networks,” in *GLOBECOM 2022-2022 IEEE Global Communications Conference*. IEEE, 2022, pp. 3272–3277.
- [31] Y. Wang, M. Chen, T. Luo, W. Saad, D. Niyato, H. V. Poor, and S. Cui, “Performance optimization for semantic communications: An attention-based reinforcement learning approach,” *IEEE Journal on Selected Areas in Communications*, vol. 40, no. 9, pp. 2598–2613, 2022.
- [32] Z. Yang, M. Chen, Z. Zhang, and C. Huang, “Energy efficient semantic communication over wireless networks with rate splitting,” *IEEE Journal on Selected Areas in Communications*, 2023.
- [33] H. Zhang, H. Wang, Y. Li, K. Long, and A. Nallanathan, “Drl-driven dynamic resource allocation for task-oriented semantic communication,” *IEEE Transactions on Communications*, vol. 71, no. 7, pp. 3992–4004, 2023.
- [34] W. Zhang, Y. Wang, M. Chen, T. Luo, and D. Niyato, “Optimization of image transmission in a cooperative semantic communication networks,” *IEEE Transactions on Wireless Communications*, 2023.

- [35] L. X. Nguyen, H. Q. Le, Y. L. Tun, P. S. Aung, Y. K. Tun, Z. Han, and C. S. Hong, "An efficient federated learning framework for training semantic communication systems," *IEEE Transactions on Vehicular Technology*, pp. 1–6, 2024.
- [36] H. Sun, H. Tian, W. Ni, and J. Zheng, "Federated learning-based cooperative model training for task-oriented semantic communication," in *IEEE Conference on Computer Communications Workshops (INFOCOM Workshops)*, 2024, pp. 1–6.
- [37] Y. Wang, W. Ni, W. Yi, X. Xu, P. Zhang, and A. Nallanathan, "Federated contrastive learning for personalized semantic communication," *IEEE Communications Letters*, vol. 28, no. 8, pp. 1875–1879, 2024.
- [38] E. Bourtsoulatzé, D. B. Kurka, and D. Gündüz, "Deep joint source-channel coding for wireless image transmission," *IEEE Transactions on Cognitive Communications and Networking*, vol. 5, no. 3, pp. 567–579, 2019.
- [39] T. Van Chien, D. X. Phuc, N. T. Hoa *et al.*, "Image restoration under semantic communications," in *2022 International Conference on Advanced Technologies for Communications (ATC)*. IEEE, 2022, pp. 332–337.
- [40] W. Yang, Z. Xiong, H. Du, Y. Yuan, and T. Q. Quek, "Semantic change driven generative semantic communication framework," in *2024 IEEE Wireless Communications and Networking Conference (WCNC)*. IEEE, 2024, pp. 01–06.
- [41] S. Luo, X. Chen, Q. Wu, Z. Zhou, and S. Yu, "HFEL: Joint edge association and resource allocation for cost-efficient hierarchical federated edge learning," *IEEE Transactions on Wireless Communications*, vol. 19, no. 10, pp. 6535–6548, 2020.
- [42] Z. Yang, M. Chen, W. Saad, C. S. Hong, and M. Shikh-Bahaei, "Energy efficient federated learning over wireless communication networks," *IEEE Transactions on Wireless Communications*, vol. 20, no. 3, pp. 1935–1949, 2020.
- [43] C. T. Dinh, N. H. Tran, M. N. Nguyen, C. S. Hong, W. Bao, A. Y. Zomaya, and V. Gramoli, "Federated learning over wireless networks: Convergence analysis and resource allocation," *IEEE/ACM Transactions on Networking*, vol. 29, no. 1, pp. 398–409, 2020.
- [44] D. Yang, W. Zhang, Q. Ye, C. Zhang, N. Zhang, C. Huang, H. Zhang, and X. Shen, "DetFed: Dynamic resource scheduling for deterministic federated learning over time-sensitive networks," *IEEE Transactions on Mobile Computing*, 2023.
- [45] X. Zhou, J. Zhao, H. Han, and C. Guet, "Joint optimization of energy consumption and completion time in federated learning," in *2022 IEEE 42nd International Conference on Distributed Computing Systems (ICDCS)*. IEEE, 2022, pp. 1005–1017.
- [46] L. Li, D. Shi, R. Hou, H. Li, M. Pan, and Z. Han, "To talk or to work: Flexible communication compression for energy efficient federated learning over heterogeneous mobile edge devices," in *IEEE Conference on Computer Communications (INFOCOM)*, 2021, pp. 1–10.
- [47] D. Huang, F. Gao, X. Tao, Q. Du, and J. Lu, "Toward semantic communications: Deep learning-based image semantic coding," *IEEE Journal on Selected Areas in Communications*, 2022.
- [48] J. Wu, C. Wu, Y. Lin, T. Yoshinaga, L. Zhong, X. Chen, and Y. Ji, "Semantic segmentation-based semantic communication system for image transmission," *Digital Communications and Networks*, 2023.
- [49] C. Dong, H. Liang, X. Xu, S. Han, B. Wang, and P. Zhang, "Innovative semantic communication system," *arXiv preprint arXiv:2202.09595*, 2022.
- [50] S. Kumari and A. Singh, "Fair end-to-end window-based congestion control in time-varying data communication networks," *International Journal of Communication Systems*, vol. 32, no. 11, p. e3986, 2019.
- [51] Z. Xiong, J. Zhao, D. Niyato, R. Deng, and J. Zhang, "Reward optimization for content providers with mobile data subsidization: A hierarchical game approach," *IEEE Transactions on Network Science and Engineering*, vol. 7, no. 4, pp. 2363–2377, 2020.
- [52] A. Cambini and L. Martein, *Generalized convexity and optimization: Theory and applications*. Springer Science & Business Media, 2008, vol. 616.
- [53] Y. Jong, "An efficient global optimization algorithm for nonlinear sum-of-ratios problem," *Optimization Online*, pp. 1–21, 2012.
- [54] K. Shen and W. Yu, "Fractional programming for communication systems—Part I: Power control and beamforming," *IEEE Transactions on Signal Processing*, vol. 66, no. 10, pp. 2616–2630, 2018.
- [55] —, "Fractional programming for communication systems—Part II: Uplink scheduling via matching," *IEEE Transactions on Signal Processing*, vol. 66, no. 10, pp. 2631–2644, 2018.
- [56] S. P. Boyd and L. Vandenberghe, *Convex optimization*. Cambridge university press, 2004.
- [57] J. Xu, T.-Y. Tung, B. Ai, W. Chen, Y. Sun, and D. D. Gündüz, "Deep joint source-channel coding for semantic communications," *IEEE Communications Magazine*, vol. 61, no. 11, pp. 42–48, 2023.
- [58] J. Park, Y. Oh, S. Kim, and Y.-S. Jeon, "Joint source-channel coding for channel-adaptive digital semantic communications," *IEEE Transactions on Cognitive Communications and Networking*, 2024.
- [59] T. Wu, Z. Chen, D. He, L. Qian, Y. Xu, M. Tao, and W. Zhang, "Cddm: Channel denoising diffusion models for wireless communications," in *GLOBECOM 2023-2023 IEEE Global Communications Conference*. IEEE, 2023, pp. 7429–7434.
- [60] J. Zhao, X. Zhou, Y. Li, and L. Qian, "Optimizing utility-energy efficiency for the metaverse over wireless networks under physical layer security," in *ACM International Symposium on Theory, Algorithmic Foundations, and Protocol Design for Mobile Networks and Mobile Computing (MobiHoc)*, 2023.
- [61] M. Zhang, Y. Li, Z. Zhang, G. Zhu, and C. Zhong, "Wireless image transmission with semantic and security awareness," *IEEE Wireless Communications Letters*, vol. 12, no. 8, pp. 1389–1393, 2023.
- [62] Z. Lyu, G. Zhu, J. Xu, B. Ai, and S. Cui, "Semantic communications for image recovery and classification via deep joint source and channel coding," *IEEE Transactions on Wireless Communications*, 2024.
- [63] X. Wang, Y. Zhang, R. Shen, Y. Xu, and F.-C. Zheng, "Drl-based energy-efficient resource allocation frameworks for uplink noma systems," *IEEE Internet of Things Journal*, vol. 7, no. 8, pp. 7279–7294, 2020.
- [64] C. Fang, T. Zhang, J. Huang, H. Xu, Z. Hu, Y. Yang, Z. Wang, Z. Zhou, and X. Luo, "A drl-driven intelligent optimization strategy for resource allocation in cloud-edge-end cooperation environments," *Symmetry*, vol. 14, no. 10, p. 2120, 2022.
- [65] M. Khani, M. M. Sadr, and S. Jamali, "Deep reinforcement learning-based resource allocation in multi-access edge computing," *Concurrency and Computation: Practice and Experience*, vol. 36, no. 15, p. e7995, 2024.
- [66] T. J. Chua, W. Yu, and J. Zhao, "Mobile edge adversarial detection for digital twinning to the metaverse: A deep reinforcement learning approach," *IEEE Transactions on Wireless Communications*, 2023.
- [67] Y. Wenhan, L. Qian, T. J. Chua, and J. Zhao, "Counterfactual reward estimation for credit assignment in multi-agent deep reinforcement learning over wireless video transmission," in *2024 IEEE 44th International Conference on Distributed Computing Systems (ICDCS)*. IEEE, 2024, pp. 1177–1189.



Yang Li (Student Member, IEEE) received his B.Eng in July 2022 from Beijing University of Posts and Telecommunications (BUPT) in China. He is currently pursuing a PhD degree in the College of Computing and Data Science (CCDS) at Nanyang Technological University (NTU), Singapore. His research interest focuses on efficiency and security in AI-driven networks, as well as privacy-preserving AI technologies.



Xinyu Zhou received her B.Eng at the department of Computer Science and Engineering from Southern University of Science and Technology (SUSTech) in 2020. She is currently a PhD student from Nanyang Technological University, Singapore. Her research interests include Optimization, Federated Learning, Wireless Communications.



Jun Zhao (S'10-M'15) is currently an Assistant Professor in the College of Computing and Data Science (CCDS) at Nanyang Technological University (NTU) in Singapore. He received a PhD degree in May 2015 in Electrical and Computer Engineering from Carnegie Mellon University (CMU) in the USA, affiliating with CMU's renowned CyLab Security & Privacy Institute, and a bachelor's degree in July 2010 from Shanghai Jiao Tong University in China.